Eur. Phys. J. C (2025) 85:18
https://doi.org/10.1140/epjc/s10052-024-13716-3

THE EUROPEAN PHYSICAL JOURNAL C

Regular Article - Theoretical Physics

Non-singular anisotropic solutions for strange star model in $f(\mathcal{R}, \mathcal{T}, \mathcal{R}_{\zeta\gamma}\mathcal{T}^{\zeta\gamma})$ gravity theory

Yihu Feng[1,a], **Tayyab Naseer**[2,3,b], **G. Mustafa**[4,c], **S. K. Maurya**[5,d]

[1] Department of Electronics and Information Engineering, Bozhou University, Bozhou 236800, Anhui, China
[2] Department of Mathematics and Statistics, The University of Lahore, 1-KM Defence Road, Lahore 54000, Pakistan
[3] Research Center of Astrophysics and Cosmology, Khazar University, 41 Mehseti Street, AZ1096 Baku, Azerbaijan
[4] Department of Physics, Zhejiang Normal University, Jinhua 321004, People's Republic of China
[5] Department of Mathematical and Physical Sciences, College of Arts and Sciences, University of Nizwa, Nizwa 616, Sultanate of Oman

Received: 28 September 2024 / Accepted: 17 December 2024

Abstract This article focuses on different anisotropic models within the framework of a specific modified $f(\mathcal{R}, \mathcal{T}, \mathcal{R}_{\zeta\gamma}\mathcal{T}^{\zeta\gamma})$ gravity theory. The study adopts a static spherically symmetric spacetime to determine the field equations for two different modified models: (i) $f(\mathcal{R}, \mathcal{T}, \mathcal{R}_{\zeta\gamma}\mathcal{T}^{\zeta\gamma}) = \mathcal{R} + \eta\mathcal{R}_{\zeta\gamma}\mathcal{T}^{\zeta\gamma}$, and (ii) $f(\mathcal{R}, \mathcal{T}, \mathcal{R}_{\zeta\gamma}\mathcal{T}^{\zeta\gamma}) = \mathcal{R}(1 + \eta\mathcal{R}_{\zeta\gamma}\mathcal{T}^{\zeta\gamma})$, where η is a constant parameter. To address the additional degrees of freedom in the field equations and obtain their corresponding unique solution, the Durgapal-Fuloria spacetime geometry and MIT bag model are utilized. Matching conditions are applied to determine unknown constants within the chosen spacetime geometry. We adopt a certain range of model parameters to analyze the physical characteristics of the developed models in the interior distribution of a particular compact star candidate 4U 1820-30. Energy conditions and some other tests are also implemented to ensure their viability and stability. Additionally, the disappearing radial pressure constraint is employed to find the values of the model parameter, aligning with the observed information of an array of stars. The study concludes that both of our models are well-behaved and satisfy all necessary conditions, and thus we observe them suitable for the modeling of astrophysical objects.

1 Introduction

The scientific community has long regarded general theory of relativity (GR) as the dominant gravitational theory, successfully tackling numerous challenges. However, it has limitations in fully explaining the rapid cosmic expansion. Recent observations have hinted at a repulsive force, known as 'dark energy', which is believed to drive galaxies apart and contribute to the cosmic acceleration. In response to various cosmic mysteries, scientists have been investigating multiple extensions to GR. The $f(\mathcal{R})$ theory represents the pioneering extension of GR achieved through modifying the action, where the Ricci scalar $\mathcal{R}$ is supplanted with the generalized function [1]. Researchers have extensively utilized various approaches in this context to investigate the feasibility of self-gravitating structures [2–6]. Moreover, $f(\mathcal{R})$ gravity models have been instrumental in addressing diverse cosmological issues, such as the late-time cosmic evolution, the inflationary epoch in which our universe grown at an exponential rate, and more [7–10], extending their applications beyond celestial bodies.

In a research endeavor led by Bertolami and colleagues [11], the quest to unveil the enigmatic aspects of the cosmos prompted an investigation into a novel concept concerning the coupling between matter and geometry. This exploration involved unifying the influence of geometry and the fluid Lagrangian in $f(\mathcal{R})$ framework. The innovative nature of this approach sparked the interest of numerous astronomers, who subsequently shifted their focus towards comprehending the accelerated expansion. Building upon these initial insights, recent advancements have given rise to modified theories, garnering significant attention in the scientific field. Harko et al. [12] proposed the first-ever theory based on this idea,

[a] e-mail: fengyihubzxy@163.com
[b] e-mail: tayyab.naseer@math.uol.edu.pk;tayyab.naseer@khazar.org; tayyabnaseer48@yahoo.com (corresponding author)
[c] e-mail: gmustafa3828@gmail.com
[d] e-mail: sunil@unizwa.edu.om (corresponding author)

Published online: 10 January 2025

termed $f(\mathcal{R},\mathcal{T})$ gravity, where $\mathcal{T}$ signifies the trace of the energy-momentum tensor (EMT) whose incorporation leads to non-conservation effects, prompting thorough analysis of the self-gravitating bodies, resulted in numerous significant discoveries [13–22]. In a related development, Haghani et al. [23] proposed another theory whose functional dependent on $\mathcal{R}_{\zeta\gamma}\mathcal{T}^{\zeta\gamma}$ along with previous two entities. They explored an epoch of cosmic expansion characterized by rapid growth and analyzed multiple models to evaluate their validity in this context. They further enhanced their analysis by employing the Lagrange multiplier method and computed conserved EMT even in this theoretical framework.

In this theory, the presence of a non-conserved EMT introduces an extra force that disrupts the motion of test particles along geodesic paths. Researchers [24] investigated two models, namely $\mathcal{R}+\eta\mathcal{R}_{\zeta\gamma}\mathcal{T}^{\zeta\gamma}$ and $\mathcal{R}(1+\eta\mathcal{R}_{\zeta\gamma}\mathcal{T}^{\zeta\gamma})$, along with different fluid Lagrangians. Their study delved into various properties related to black holes and the corresponding laws to discuss their thermodynamics. Odintsov and Sáez-Gómez [25] discussed the effects of varying fluid configurations, demonstrating that such alternations can result in a pure de Sitter model within this modified framework. Additionally, Ayuso et al. [26] analyzed the field equations in this extended theory through the incorporation of some fields (either scalar or vector), revealing the presence of non-linear terms arising from such couplings between fluid and geometry. The work presented in [27] extensively delves into the stability checks for various models through the incorporation of perturbation functions. A crucial observation was made regarding the impact of the matter Lagrangian density, particularly in relation to the radial and tangential components of pressure [28]. Additionally, the decomposition of the curvature tensor resulted in scalar functions relevant to the fluids possessing charge/uncharge properties, bearing importance in studying celestial systems [29–34]. Through diverse techniques, solutions to modified field equations were extracted, leading to the modeling of several anisotropic systems that proved consistent and physically valid results [35,36].

The reigning factors which define the self-gravitating interiors, does not matter which properties they exhibit, are commonly the energy density and pressure (same or different in different directions depending on the nature of the fluid). These elements are interconnected in specific ways, one of them being the MIT equation of state (EoS) [37]. It is worth noting that this model effectively grabs the features of the objects composed of quark-like elements such as RXJ 185635-3754, 4U 1820-30, PSR 0943+10, 4U 1728-34, SAX J 1808.4-3658, Her X-1, among others. Conversely, such characterization is not achievable using a neutron star EoS [38]. Researchers have utilized the same model to explore the internal configuration of strange stars [39–43]. Demorest with his colleagues [44] conducted a comprehensive exploration of the massive system PSR J1614-2230, determining that only the MIT model can account for such extraordinarily dense bodies. Rahaman et al. [45] described in more depth some particular stellar interiors using the same model. Similarly, various researchers expanded upon this research by investigating various modified gravity scenarios, leading to the identification of physically stable models [46,47].

This paper is focused on assessing the viability of the Durgapal–Fuloria models coupled with anisotropic pressure in the $f(\mathcal{R},\mathcal{T},\mathcal{R}_{\zeta\gamma}\mathcal{T}^{\zeta\gamma})$ framework. The following lines explain the organization of the current paper. In the next section, we introduce some fundamental definitions and calculate the field equations for a couple of modified models. Furthermore, we utilize the MIT bag model to describe the inner structure of the quark-like structures. Section 3 employs matching criteria to determine a doublet (d_1, d_2) appearing due to the consideration of Durgapal–Fuloria metric. Moving to Sect. 4, we conduct a graphical analysis of different properties of the obtained fluid determinants by fixing the model parameter. After this, we identify the model parameter that align with the calculated data of various stars in Sect. 5. Finally, the last section presents a brief summary regarding our results.

2 Modified theory and field equations

The modified Einstein–Hilbert action with $\kappa = 8\pi$ takes the form [25]

$$S=\int\sqrt{-g}\left\{\frac{f(\mathcal{R},\mathcal{T},\mathcal{R}_{\zeta\gamma}\mathcal{T}^{\zeta\gamma})}{16\pi}+Ł_m\right\}d^4x, \tag{1}$$

where $Ł_m$ being the matter's Lagrangian density. We apply the least-action principle on the above equation, resulting in

$$\mathcal{G}_{\zeta\gamma}=8\pi\mathcal{T}^{(\mathrm{ef})}_{\zeta\gamma}=\frac{8\pi\mathcal{T}_{\zeta\gamma}}{f_{\mathcal{R}}-Ł_m f_{\mathcal{Q}}}+\mathcal{T}^{(\mathrm{cr})}_{\zeta\gamma}, \tag{2}$$

which relates the effective matter distribution and geometry expressed by the EMT $\mathcal{T}^{(\mathrm{eff})}_{\zeta\gamma}$ and the Einstein tensor $\mathcal{G}_{\zeta\gamma}$, respectively. Also, $\mathcal{Q}=\mathcal{R}_{\zeta\gamma}\mathcal{T}^{\zeta\gamma}$. The insertion of generalized functional f in Eq. (1) produces some additional terms along with the fluid distribution of GR, and we represent it by $\mathcal{T}^{(\mathrm{cr})}_{\zeta\gamma}$. Its expression is

$$\begin{aligned}\mathcal{T}^{(\mathrm{cor})}_{\zeta\gamma}=&-\frac{1}{\left(Ł_m f_{\mathcal{Q}}-f_{\mathcal{R}}\right)}\Bigg[\left(f_{\mathcal{T}}+\frac{1}{2}\mathcal{R}f_{\mathcal{Q}}\right)\mathcal{T}_{\zeta\gamma}-\Bigg\{Ł_m f_{\mathcal{T}}\\&-\frac{\mathcal{R}}{2}\left(\frac{f}{\mathcal{R}}-f_{\mathcal{R}}\right)+\frac{1}{2}\nabla_\varrho\nabla_\sigma(f_{\mathcal{Q}}\mathcal{T}^{\varrho\sigma})\Bigg\}g_{\zeta\gamma}\\&-\frac{1}{2}\Box(f_{\mathcal{Q}}\mathcal{T}_{\zeta\gamma})-(g_{\zeta\gamma}\Box-\nabla_\zeta\nabla_\gamma)f_{\mathcal{R}}\\&-2f_{\mathcal{Q}}\mathcal{R}_{\varrho(\zeta}\mathcal{T}^{\varrho}_{\gamma)}+\nabla_\varrho\nabla_{(\zeta}[\mathcal{T}^{\varrho}_{\gamma)}f_{\mathcal{Q}}]\end{aligned}$$

$$+2(f_{\mathcal{Q}}\mathcal{R}^{\varrho\sigma}+f_{\mathcal{T}}g^{\varrho\sigma})\frac{\partial^2\text{Ł}_m}{\partial g^{\zeta\gamma}\partial g^{\varrho\sigma}}\Bigg], \tag{3}$$

where the partial derivatives $f_{\mathcal{R}}$, $f_{\mathcal{T}}$ and $f_{\mathcal{Q}}$ are involved that differentiate the functional with respect to its arguments. Two other mathematical symbols are used, known as the covariant derivative (∇_ϱ) and and D'Alambert operator $\left(\Box\equiv\frac{1}{\sqrt{-g}}\partial_\zeta(\sqrt{-g}g^{\zeta\gamma}\partial_\gamma)\right)$. It has been observed in the literature that the fluid Lagrangian takes the value $\text{Ł}_m=-\mu$ (μ being the energy density) in this theory to produce well-behaving results. On the other hand, we also observe that the equivalence principle is not satisfied in the current scenario (i.e., $\nabla_\zeta\mathcal{T}^{\zeta\gamma}\neq 0$), so an extra force must be required to make the system in stable equilibrium. Such kind of force alters the geodesic motion of the particles in spacetime regions. Mathematical, this force becomes

$$\begin{aligned}\nabla^\zeta\mathcal{T}_{\zeta\gamma}=\frac{2}{2f_{\mathcal{T}}+\mathcal{R}f_{\mathcal{Q}}+16\pi}\Bigg[&\nabla_\zeta\left(f_{\mathcal{Q}}\mathcal{R}^{\varrho\zeta}\mathcal{T}_{\varrho\gamma}\right)\\&-\mathcal{G}_{\zeta\gamma}\nabla^\zeta\left(f_{\mathcal{Q}}\text{Ł}_m\right)+\nabla_\gamma\left(\text{Ł}_m f_{\mathcal{T}}\right)\\&-\frac{1}{2}\nabla_\gamma\mathcal{T}^{\varrho\sigma}\left(f_{\mathcal{T}}g_{\varrho\sigma}+f_{\mathcal{Q}}\mathcal{R}_{\varrho\sigma}\right)\\&-\frac{1}{2}\left\{\nabla^\zeta(\mathcal{R}f_{\mathcal{Q}})+2\nabla^\zeta f_{\mathcal{T}}\right\}\mathcal{T}_{\zeta\gamma}\Bigg].\end{aligned} \tag{4}$$

The EMT plays a crucial role in examining the internal properties of self-gravitating systems, which is vital in the realm of astrophysics. In this field, a diverse array of cosmic entities is thought to display the anisotropy in pressure. This makes the EMT an indispensable tool for studying the complex processes of stellar evolution. The mathematical expression of the anisotropic EMT is as follows

$$\mathcal{T}_{\zeta\gamma}=(\mu+P_\perp)\mathrm{U}_\zeta\mathrm{U}_\gamma+P_\perp g_{\zeta\gamma}+(P_r-P_\perp)\mathrm{V}_\zeta\mathrm{V}_\gamma, \tag{5}$$

where $P_\perp$ is the tangential pressure, V_ζ indicates the four-vector, P_r being the radial pressure and U_ζ represents the four-velocity. The trace of Eq. (2) along with (3) is

$$\begin{aligned}&3\nabla^\varrho\nabla_\varrho f_{\mathcal{R}}-\mathcal{T}(8\pi+f_{\mathcal{T}})-\mathcal{R}\left(\frac{\mathcal{T}}{2}f_{\mathcal{Q}}-f_{\mathcal{R}}\right)\\&+\frac{1}{2}\nabla^\varrho\nabla_\varrho(f_{\mathcal{Q}}\mathcal{T})+\nabla_\zeta\nabla_\varrho(f_{\mathcal{Q}}\mathcal{T}^{\zeta\varrho})\\&-2f+(\mathcal{R}f_{\mathcal{Q}}+4f_{\mathcal{T}})\text{Ł}_m+2\mathcal{R}_{\zeta\varrho}\mathcal{T}^{\zeta\varrho}f_{\mathcal{Q}}\\&-2g^{\gamma\sigma}\frac{\partial^2\text{Ł}_m}{\partial g^{\gamma\sigma}\partial g^{\zeta\varrho}}\left(f_{\mathcal{T}}g^{\zeta\varrho}+f_{\mathcal{Q}}R^{\zeta\varrho}\right)=0.\end{aligned}$$

The metric or spacetime is a fundamental concept that enables us to investigate the gravitational field and its effects on the curvature of spacetime within heavily celestial objects. In this context, we focus on the interior spherical spacetime that is described by the line element given as

$$ds^2=e^{A_1}dr^2+r^2d\theta^2+r^2\sin^2\theta d\phi^2-e^{A_0}dt^2, \tag{6}$$

where $A_0=A_0(r)$ and $A_1=A_1(r)$. The quantities used in Eq. (5) are now become

$$\mathrm{V}^\zeta=\delta^\zeta_1e^{-\frac{A_1}{2}},\quad \mathrm{U}^\zeta=\delta^\zeta_0e^{-\frac{A_0}{2}}, \tag{7}$$

satisfying $\mathrm{V}^\zeta\mathrm{U}_\zeta=0$ and $\mathrm{U}^\zeta\mathrm{U}_\zeta=-1$.

Our cosmos is currently experiencing a period of rapid expansion and is filled with a multitude of stars that exist within a non-linear context. Despite this non-linearity, conducting analyzes using linear methods offer a better understanding of the formation and behavior of these heavily structures. To delve into this, we explore following two models as [23].

Model 1: $f(\mathcal{R},\mathcal{T},\mathcal{R}_{\zeta\gamma}\mathcal{T}^{\zeta\gamma})=\mathcal{R}+\eta\mathcal{R}_{\zeta\gamma}\mathcal{T}^{\zeta\gamma}$,

Model 2: $f(\mathcal{R},\mathcal{T},\mathcal{R}_{\zeta\gamma}\mathcal{T}^{\zeta\gamma})=\mathcal{R}(1+\eta\mathcal{R}_{\zeta\gamma}\mathcal{T}^{\zeta\gamma})$,

where η being the arbitrary parameter. It is important to highlight that different parametric values, all falling within the estimated range, guarantee the validity of stars. Haghani et al. [23] conducted a thorough examination of these models, delving into the evolution of the scale factor and deceleration parameter. Similarly, Sharif and Zubair [24] focused on isotropic configurations within the same context, deriving acceptable values for the respective parameters. The expression for the last term in above models can be expressed as

$$\begin{aligned}&\mathcal{R}_{\zeta\gamma}\mathcal{T}^{\zeta\gamma}\\&=e^{-A_1}\Bigg[\frac{\mu}{4}\left(A_0'^2-A_0'A_1'+2A_0''+\frac{4A_0'}{r}\right)\\&+P_\perp\left(\frac{A_1'}{r}-\frac{A_0'}{r}+\frac{2e^{A_1}}{r^2}-\frac{2}{r^2}\right)\\&-\frac{P_r}{4}\left(A_0'^2-A_0'A_1'+2A_0''+\frac{4A_1'}{r}\right)\Bigg],\end{aligned}$$

where $'=\frac{\partial}{\partial r}$.

The field equations (2) characterizing the anisotropic interior (5) are given for **Model 1** as

$$\begin{aligned}8\pi\mu=e^{-A_1}\Bigg[&\frac{A_1'}{r}+\frac{e^{A_1}}{r^2}-\frac{1}{r^2}\\&+\eta\Bigg\{\mu\left(\frac{3A_0'A_1'}{8}-\frac{A_0'^2}{8}+\frac{A_1'}{r}+\frac{e^{A_1}}{r^2}\right.\\&\left.-\frac{3A_0''}{4}-\frac{3A_0'}{2r}-\frac{1}{r^2}\right)-\mu'\left(\frac{A_1'}{4}-\frac{1}{r}-A_0'\right)\\&+\frac{\mu''}{2}+P_r\left(\frac{A_0'A_1'}{8}-\frac{A_0'^2}{8}-\frac{A_0''}{4}+\frac{A_1'}{2r}+\frac{A_1''}{2}\right.\\&\left.-\frac{3A_1'^2}{4}\right)+\frac{5A_1'P_r'}{4}-\frac{P_r''}{2}\\&+P_\perp\left(\frac{A_1'}{2r}-\frac{A_0'}{2r}+\frac{3e^{A_1}}{r^2}-\frac{1}{r^2}\right)-\frac{P_\perp'}{r}\Bigg\}\Bigg],\end{aligned} \tag{8}$$

$$
\begin{aligned}
8\pi P_r &= e^{-A_1}\Bigg[\frac{A_0'}{r}-\frac{e^{A_1}}{r^2}+\frac{1}{r^2}\\
&\quad+\eta\Bigg\{\mu\Bigg(\frac{A_0'A_1{}'}{8}+\frac{A_0'^2}{8}-\frac{A_0''}{4}-\frac{A_0'}{2r}\Bigg)-\frac{A_0'\mu'}{4}-P_r\\
&\quad\times\Bigg(\frac{5A_0'^2}{8}-\frac{7A_0'A_1{}'}{8}+\frac{5A_0''}{4}-\frac{7A_1{}'}{2r}\\
&\quad+\frac{A_0'}{r}-A_1{}'^2-\frac{e^{A_1}}{r^2}+\frac{1}{r^2}\Bigg)+P_r'\Bigg(\frac{A_0'}{4}+\frac{1}{r}\Bigg)\\
&\quad-P_\perp\Bigg(\frac{A_1{}'}{2r}-\frac{A_0'}{2r}+\frac{3e^{A_1}}{r^2}-\frac{1}{r^2}\Bigg)+\frac{P_\perp'}{r}\Bigg\}\Bigg],\\
8\pi P_\perp &= e^{-A_1}\Bigg[\frac{A_0'^2}{4}-\frac{A_0'A_1{}'}{4}+\frac{A_0''}{2}-\frac{A_1{}'}{2r}+\frac{A_0'}{2r}\\
&\quad+\eta\Bigg\{\mu\Bigg(\frac{A_0'^2}{8}+\frac{A_0'A_1{}'}{8}-\frac{A_0''}{4}-\frac{A_0'}{2r}\Bigg)\\
&\quad-\frac{A_0'\mu'}{4}+P_r\Bigg(\frac{A_0'^2}{8}-\frac{A_0'A_1{}'}{8}\\
&\quad+\frac{A_0''}{4}-\frac{A_1{}'}{2r}-\frac{A_1{}''}{2}+\frac{3A_1{}'^2}{4}\Bigg)-\frac{5A_1{}'P_r'}{4}+\frac{P_r''}{2}
\end{aligned}
\tag{9}
$$

$$
\begin{aligned}
&\quad-P_\perp\Bigg(\frac{A_0'^2}{4}-\frac{A_0'A_1{}'}{4}+\frac{A_0''}{2}\\
&\quad-\frac{A_1{}'}{r}+\frac{A_0'}{r}\Bigg)-P_\perp'\Bigg(\frac{A_1{}'}{4}-\frac{A_0'}{4}\\
&\quad-\frac{3}{r}\Bigg)+\frac{P_\perp''}{2}\Bigg\}\Bigg].
\end{aligned}
\tag{10}
$$

Similarly, expressions for matter variables corresponding to **Model 2** as

$$
\begin{aligned}
8\pi\mu &= e^{-A_1}\Bigg[\frac{A_1{}'}{r}+\frac{e^{A_1}}{r^2}-\frac{1}{r^2}+\eta\Bigg\{\mu\Bigg(\Bigg(\frac{A_1{}'}{r}+\frac{e^{A_1}}{r^2}\\
&\quad-\frac{1}{r^2}\Bigg)\alpha_1-\mathcal{R}\Bigg(\frac{1}{r^2}-\frac{A_1{}'}{r}-\frac{e^{A_1}}{r^2}\\
&\quad+\frac{\mathcal{R}e^{A_1}}{2}-\frac{3A_0'^2}{8}\\
&\quad-\frac{3A_0'}{2r}+\frac{5A_0'A_1{}'}{8}-\frac{3A_0''}{4}\Bigg)+\mathcal{R}'\Bigg(\frac{A_1{}'}{2}-\frac{1}{r}\Bigg)\\
&\quad-\frac{\mathcal{R}''}{2}-\alpha_4\Bigg(\frac{2}{r}-\frac{A_1{}'}{2}\Bigg)-\alpha_7\Bigg)\\
&\quad+\mu'\Bigg(\alpha_1\Bigg(\frac{A_1{}'}{2}-\frac{2}{r}\Bigg)-\mathcal{R}\Bigg(\frac{1}{r}\\
&\quad-\frac{A_1{}'}{4}\Bigg)-\mathcal{R}'-2\alpha_4\Bigg)-\mu''\Bigg(\alpha_1\\
&\quad+\frac{\mathcal{R}}{2}\Bigg)-P_r\Bigg(\Bigg(\frac{1}{r^2}-\frac{A_1{}'}{r}\\
&\quad-\frac{e^{A_1}}{r^2}\Bigg)\alpha_2+\mathcal{R}\Bigg(\frac{A_0'^2}{8}-\frac{1}{r^2}-\frac{A_0'A_1{}'}{8}+\frac{A_1{}'}{2r}+\frac{A_0''}{4}\Bigg)\\
&\quad-\mathcal{R}'\Bigg(\frac{2}{r}-\frac{A_1{}'}{2}\Bigg)\\
&\quad-\frac{\mathcal{R}''}{2}+\alpha_5\Bigg(\frac{2}{r}-\frac{A_1{}'}{2}\Bigg)+\alpha_8\Bigg)-P_r'\Bigg(\alpha_2\Bigg(\frac{2}{r}-\frac{A_1{}'}{2}\Bigg)+\mathcal{R}\\
&\quad\times\Bigg(\frac{A_1{}'}{4}-\frac{2}{r}\Bigg)\\
&\quad-\mathcal{R}'+2\alpha_5\Bigg)-P_r''\Bigg(\alpha_2-\frac{\mathcal{R}}{2}\Bigg)-P_\perp\Bigg(\Bigg(\frac{1}{r^2}\\
&\quad-\frac{A_1{}'}{r}-\frac{e^{A_1}}{r^2}\Bigg)\alpha_3\\
&\quad+\mathcal{R}\Bigg(\frac{A_0'}{2r}+\frac{1}{r^2}-\frac{A_1{}'}{2r}\Bigg)\\
&\quad+\frac{\mathcal{R}'}{r}+\alpha_6\Bigg(\frac{2}{r}-\frac{A_1{}'}{2}\Bigg)\\
&\quad+\alpha_9\Bigg)-P_\perp'\Bigg(\alpha_3\Bigg(\frac{2}{r}-\frac{A_1{}'}{2}\Bigg)\\
&\quad+\frac{\mathcal{R}}{2}+2\alpha_6\Bigg)-P_\perp''\alpha_3\Bigg\}\Bigg],
\end{aligned}
\tag{11}
$$

$$
\begin{aligned}
8\pi P_r &= e^{-A_1}\Bigg[\frac{A_0'}{r}-\frac{e^{A_1}}{r^2}\\
&\quad+\frac{1}{r^2}+\eta\Bigg\{\mu\Bigg(\Bigg(\frac{A_0'}{r}-\frac{e^{A_1}}{r^2}+\frac{1}{r^2}\Bigg)\alpha_1\\
&\quad-\mathcal{R}\Bigg(\frac{e^{A_1}}{r^2}-\frac{1}{r^2}-\frac{A_0'}{r}+\frac{A_0'^2}{8}+\frac{A_0'}{2r}\\
&\quad-\frac{A_0'A_1{}'}{8}+\frac{A_0''}{4}\Bigg)+\frac{\mathcal{R}'A_0'}{4}+\alpha_4\Bigg(\frac{2}{r}+\frac{A_0'}{2}\Bigg)\Bigg)\\
&\quad+\mu'\Bigg(\alpha_1\Bigg(\frac{2}{r}+\frac{A_0'}{2}\Bigg)\\
&\quad+\frac{\mathcal{R}A_0'}{4}\Bigg)+P_r\Bigg(\Bigg(\frac{1}{r^2}\\
&\quad+\frac{A_0'}{r}-\frac{e^{A_1}}{r^2}\Bigg)\alpha_2-\mathcal{R}\Bigg(\frac{\mathcal{R}e^{A_1}}{2}-\frac{3A_0'^2}{8}\\
&\quad+\frac{1}{r^2}+\frac{A_0'}{r}+\frac{3A_1{}'}{2r}+\frac{3A_0'A_1{}'}{8}-\frac{3A_0''}{4}\Bigg)\\
&\quad-\mathcal{R}'\Bigg(\frac{1}{r}+\frac{A_0'}{4}\Bigg)+\alpha_5\Bigg(\frac{2}{r}+\frac{A_0'}{2}\Bigg)\Bigg)\\
&\quad+P_r'\Bigg(\alpha_2\Bigg(\frac{2}{r}+\frac{A_0'}{2}\Bigg)-\mathcal{R}\Bigg(\frac{A_0'}{4}+\frac{1}{r}\Bigg)\Bigg)-P_\perp\Bigg(\Bigg(\frac{A_0'}{r}\\
&\quad+\frac{e^{A_1}}{r^2}-\frac{1}{r^2}\Bigg)\alpha_3+\mathcal{R}\Bigg(\frac{A_1{}'}{2r}-\frac{1}{r^2}-\frac{A_0'}{2r}\Bigg)+\frac{\mathcal{R}'}{r}\\
&\quad-\alpha_6\Bigg(\frac{2}{r}+\frac{A_0'}{2}\Bigg)\Bigg)\\
&\quad+P_\perp'\Bigg(\alpha_3\Bigg(\frac{2}{r}+\frac{A_0'}{2}\Bigg)-\frac{\mathcal{R}}{2}\Bigg)\Bigg\}\Bigg],\\
8\pi P_\perp &= e^{-A_1}\Bigg[\frac{A_0''}{2}-\frac{A_0'A_1{}'}{4}+\frac{A_0'^2}{4}+\frac{A_0'}{2r}-\frac{A_1}{2r}\\
&\quad+\eta\Bigg\{\mu\Bigg(\alpha_1\Bigg(\frac{A_0''}{2}-\frac{A_0'A_1{}'}{4}+\frac{A_0'^2}{4}\\
&\quad+\frac{A_0'}{2r}-\frac{A_1}{2r}\Bigg)-\mathcal{R}\Bigg(\frac{A_0'A_1{}'}{8}-\frac{A_0''}{4}-\frac{A_0'^2}{8}+\frac{A_1{}'}{2r}\Bigg)\\
&\quad-\Bigg(\frac{A_1{}'}{2}-\frac{1}{r}-\frac{A_0'}{2}\Bigg)\alpha_4+\alpha_7
\end{aligned}
\tag{12}
$$

$$
\begin{aligned}
&- \frac{\mathcal{R}' A_0'}{4}\Big) - \mu'\Big(\alpha_1\Big(\frac{A_1'}{2} \\
&- \frac{1}{r} - \frac{A_0'}{2}\Big) + \frac{\mathcal{R}A_0'}{4} - 2\alpha_4\Big) + \mu''\alpha_1 - P_r\Big(\Big(\frac{A_1'}{2r} \\
&- \frac{A_0''}{2} - \frac{A_0'^2}{4} - \frac{A_0'}{2r} + \frac{A_0'A_1'}{4}\Big)\alpha_2 \\
&+ \mathcal{R}\Big(\frac{A_0'^2}{8} + \frac{A_0'}{2r} - \frac{A_0'A_1'}{8} + \frac{A_0''}{4}\Big) + \mathcal{R}' \\
&\times \Big(\frac{A_0'}{2} + \frac{1}{r} - \frac{A_1'}{4}\Big) + \frac{\mathcal{R}''}{2} \\
&+ \alpha_5\Big(\frac{A_1'}{2} - \frac{1}{r} - \frac{A_0'}{2}\Big) - \alpha_8\Big) - P_r'\Big(\alpha_2\Big(\frac{A_1'}{2} \\
&- \frac{1}{r} - \frac{A_0'}{2}\Big) + \mathcal{R}\Big(\frac{A_0'}{2} + \frac{1}{r} - \frac{A_1'}{4}\Big) \\
&+ \mathcal{R}' - 2\alpha_5\Big) + P_r''\Big(\alpha_2 - \frac{\mathcal{R}}{2}\Big) + P_\perp\Big(\alpha_3 \\
&\times \Big(\frac{A_0''}{2} - \frac{A_0'A_1'}{4} + \frac{A_0'^2}{4} + \frac{A_0'}{2r} \\
&- \frac{A_1}{2r}\Big) - \mathcal{R}\Big(\frac{\mathcal{R}e^{A_1}}{2} - \frac{2}{r^2} + \frac{A_1'}{r} - \frac{A_0'}{r} + \frac{2e^{A_1}}{r^2}\Big) \\
&- \mathcal{R}'\Big(\frac{A_0'}{4} - \frac{A_1'}{4}\Big) - \frac{\mathcal{R}''}{2} \\
&- \alpha_6\Big(\frac{A_1'}{2} - \frac{1}{r} - \frac{A_0'}{2}\Big) + \alpha_9\Big) \\
&- P_\perp'\Big(\alpha_3\Big(\frac{A_1'}{2} - \frac{1}{r} \\
&- \frac{A_0'}{2}\Big) + \mathcal{R}\Big(\frac{A_0'}{4} - \frac{A_1'}{4} \\
&+ \frac{2}{r}\Big) + \mathcal{R}' - 2\alpha_6\Big) + P_\perp''\Big(\alpha_3 - \frac{\mathcal{R}}{2}\Big)\Big\}\Big], \qquad (13)
\end{aligned}
$$

where $\alpha_j^{'s}$, ($j = 1$ to 9) are presented in Appendix A. A formula for calculating the spherical mass distribution has been calculated [48], represented as

$$m(r) = \frac{r}{2}\big(1 - g^{\xi\gamma} r_{,\xi} r_{,\gamma}\big),$$

simplifies to

$$m(r) = \frac{r}{2}\big(1 - e^{-A_1}\big). \qquad (14)$$

The two sets of differential equations (8)–(10) and (11)–(13) involve matter determinants and their derivatives, making it a challenging task to obtain their solutions. Therefore, it becomes imperative to impose some constraints in order to derive the required solutions. In this context, we consider the MIT bag model to quark's interior [37]. The corresponding EoS is defined as

$$P_r = \frac{1}{3}\left(\mu - 4B_c\right). \qquad (15)$$

Researchers have conducted investigations into various quark interiors using the aforementioned equation and calculated values for B_c that are consistent with observed data [49,50].

After combining Eqs. (8) and (9) with (15), the explicit form of matter variables μ, P_r and P_t for **Model 1** can be expressed by

$$
\begin{aligned}
\mu = &\Big[\eta\Big(\frac{9A_0''}{8} - \frac{e^{A_1}}{r^2} + \frac{1}{r^2} \\
&- \frac{A_1''}{8} - \frac{5A_0'A_1'}{8} - \frac{A_1'^2}{16} - \frac{7A_1'}{2r} + \frac{3A_0'^2}{16} + \frac{7A_0'}{4r}\Big) \\
&+ 8\pi e^{A_1}\Big]^{-1}\Big[\frac{3}{4}\Big(\frac{A_1'}{r} \\
&+ \frac{A_0'}{r}\Big) + B_c\Big\{8\pi e^{A_1} - \eta\Big(\frac{4A_1'}{r} - \frac{3A_0'^2}{4} - \frac{3A_0''}{2} + \frac{A_1''}{2} \\
&+ \frac{A_1'^2}{4} + A_0'A_1' - \frac{A_0'}{r} + \frac{e^{A_1}}{r^2} - \frac{1}{r^2}\Big)\Big\}\Big], \qquad (16)
\end{aligned}
$$

$$
\begin{aligned}
P_r = &\Big[\eta\Big(\frac{9A_0''}{8} - \frac{e^{A_1}}{r^2} + \frac{1}{r^2} \\
&- \frac{A_1''}{8} - \frac{5A_0'A_1'}{8} - \frac{A_1'^2}{16} - \frac{7A_1'}{2r} + \frac{3A_0'^2}{16} + \frac{7A_0'}{4r}\Big) \\
&+ 8\pi e^{A_1}\Big]^{-1}\Big[\frac{1}{4}\Big(\frac{A_1'}{r} + \frac{A_0'}{r}\Big) - B_c\Big\{8\pi e^{A_1} \\
&- \eta\Big(\frac{A_0'A_1'}{2} + \frac{A_1'}{r} - \frac{2A_0'}{r} \\
&+ \frac{e^{A_1}}{r^2} - A_0'' - \frac{1}{r^2}\Big)\Big\}\Big]. \qquad (17)
\end{aligned}
$$

On the other hand, Eqs. (11) and (12) along with EOS (g14a) give the expressions for **Model 2**

$$
\begin{aligned}
\mu = &\Big[\eta\Big\{\frac{3}{4}\Big(\frac{A_1'}{r} + \frac{A_0'}{r}\Big)\Big(\alpha_1 \\
&+ \frac{\alpha_2}{3}\Big) + \frac{3}{8}(A_1' + A_0')\Big(\alpha_4 + \frac{\alpha_5}{3}\Big) + \mathcal{R}\Big(\frac{A_0''}{2} + \frac{A_1'}{4r} \\
&- \frac{7A_0'A_1'}{16} + \frac{A_0'^2}{16} + \frac{5A_0'}{4r} \\
&- \frac{\mathcal{R}e^{A_1}}{2}\Big) + \mathcal{R}'\Big(\frac{A_0'}{8} - \frac{1}{2r} + \frac{A_1'}{8}\Big) - \frac{\mathcal{R}''}{4} - \frac{\alpha_8}{4}\Big\} \\
&- 8\pi e^{A_1}\Big]^{-1}\Big[-\frac{3}{4}\Big(\frac{A_1'}{r} + \frac{A_0'}{r}\Big) - 8\pi B_c e^{A_1} \\
&- \eta B_c\Big\{\Big(\frac{A_1'}{r} + \frac{A_0'}{r}\Big)\alpha_2 - \mathcal{R}\Big(\frac{A_0'^2}{2} \\
&+ \frac{\mathcal{R}e^{A_1}}{2} + \frac{A_0'}{r} + \frac{A_0'A_1'}{4} + \frac{2A_1'}{r} - \frac{A_0''}{2}\Big) \\
&- \mathcal{R}'\Big(\frac{A_0'}{4} - \frac{1}{r} + \frac{A_1'}{4}\Big) + \frac{\mathcal{R}''}{2} - \alpha_8 \\
&+ \alpha_5\Big(\frac{A_1'}{2} + \frac{A_0'}{2}\Big)\Big\}\Big], \qquad (18)
\end{aligned}
$$

$$P_r = \Big[\eta\Big\{\frac{3}{4}\Big(\frac{A_1'}{r} + \frac{A_0'}{r}\Big)$$

$$\times\left(\alpha_1+\frac{\alpha_2}{3}\right)+\frac{3}{8}\left(A_1{}'+A_0'\right)\left(\alpha_4+\frac{\alpha_5}{3}\right)$$
$$+\mathcal{R}\left(\frac{A_0''}{2}+\frac{A_1{}'}{4r}-\frac{7A_0'A_1{}'}{16}+\frac{A_0'^2}{16}+\frac{5A_0'}{4r}\right.$$
$$\left.-\frac{\mathcal{R}e^{A_1}}{2}\right)+\mathcal{R}'\left(\frac{A_0'}{8}-\frac{1}{2r}+\frac{A_1{}'}{8}\right)-\frac{\mathcal{R}''}{4}-\frac{\alpha_8}{4}\Bigg\}$$
$$-8\pi e^{A_1}\Bigg]^{-1}\Bigg[-\frac{1}{4}\left(\frac{A_1{}'}{r}+\frac{A_0'}{r}\right)+8\pi B_c e^{A_1}$$
$$-\eta B_c\Bigg\{\left(\frac{A_1{}'}{r}+\frac{A_0'}{r}\right)\alpha_1+\mathcal{R}\left(\frac{A_0'^2}{4}\right.$$
$$\left.-\frac{\mathcal{R}e^{A_1}}{2}+\frac{A_1{}'}{r}-\frac{A_0'A_1{}'}{2}+\frac{A_0''}{2}+\frac{2A_0'}{r}\right)$$
$$+\mathcal{R}'\left(\frac{A_0'}{4}-\frac{1}{r}+\frac{A_1{}'}{4}\right)-\frac{\mathcal{R}''}{2}-\alpha_7$$
$$+\alpha_4\left(\frac{A_1{}'}{2}+\frac{A_0'}{2}\right)\Bigg\}\Bigg]. \tag{19}$$

Moreover, we avoid writing an expression for tangential pressure (P_t) for both models due to the very long expression. But, we can determine the tangential pressure corresponding to **Model 1**, one can put Eqs. (16) and (17) into (10). For the **Model 2**, it can be achieved using Eqs. (13), (18) and (19).

3 A particular Ansatz and implementation of matching criteria

Given that the equations of motion possess additional unknowns till now, we shift our focus to a particular metric, i.e., Durgapal–Fuloria spacetime, that has attracted significant interest among astrophysicists. The components of this metric are provided as [51]

$$e^{A_0}=d_1\left(d_2r^2+1\right)^4,\quad e^{A_1}=\frac{7\left(d_2r^2+1\right)^2}{7-d_2^2r^4-10d_2r^2}, \tag{20}$$

involving a doublet constant (d_1, d_2) and we need to calculate its values. In our analysis, we shall utilize matching criteria to ascertain these values. Given the variety of metrics proposed in the literature, it is essential to verify the physical acceptability of the ansatz under consideration. For this purpose, a specific criterion has been suggested [52,53], which involves taking derivatives of both the time and radial components to validate its suitability, as outlined below

$$A_0'(r)=\frac{8d_2r}{d_2r^2+1},\quad A_0''(r)=\frac{8d_2}{d_2r^2+1}-\frac{16d_2^2r^2}{\left(d_2r^2+1\right)^2},$$
$$A_1{}'(r)=\frac{16d_2r\left(d_2r^2-3\right)}{\left(d_2r^2+1\right)\left(d_2^2r^4+10d_2r^2-7\right)},$$
$$A_1{}''(r)=\frac{16d_2\left(21-3d_2^4r^8+4d_2^3r^6+102d_2^2r^4-12d_2r^2\right)}{\left(d_2r^2+1\right)^2\left(d_2^2r^4+10d_2r^2-7\right)^2},$$

from which we notice that $A_0'(0)=0=A_1{}'(0)$ and $A_0''(0)$, $A_1{}''(0)>0$ in the whole domain ($r=0$ is the star's core). Hence, the considered ansatz is found to be acceptable.

The matching of the inner and outer sectors at the hypersurface provides multiple conditions that serve as a valuable tool for comprehending the structure of massive bodies. In this context, the Schwarzschild metric describing the exterior geometry is considered that has the form

$$ds^2=\frac{dr^2}{\left(1-\frac{2\mathrm{M}}{r}\right)}+r^2d\theta^2+r^2\sin^2\theta d\phi^2-\left(1-\frac{2\mathrm{M}}{r}\right)dt^2, \tag{21}$$

where M being the total exterior mass. We use only the first fundamental form of these constraints, ensuring that metric components of both geometries are continuous across the boundary. This leads to

$$g_{tt}\overset{\Sigma}{=}e^{A_0(R)}=d_1\left(d_2R^2+1\right)^4=1-\frac{2\mathrm{M}}{R}, \tag{22}$$
$$g_{rr}\overset{\Sigma}{=}e^{A_1(R)}=\frac{7\left(d_2R^2+1\right)^2}{7-d_2^2R^4-10d_2R^2}=\left(1-\frac{2\mathrm{M}}{R}\right)^{-1}. \tag{23}$$

Equations (22) and (23) simultaneously provide these two constants as

$$d_1=\frac{R-2\mathrm{M}}{R\left(d_2R^2+1\right)^4}, \tag{24}$$
$$d_2=\frac{6R^3-7\mathrm{M}R^2-2\sqrt{9R^6-14\mathrm{M}R^5}}{7\mathrm{M}R^4-4R^5}. \tag{25}$$

4 Exploring stellar solutions through graphical analysis

We devoted this section to graphically analyzing the resulting models for a particular object, namely 4U 1820-30. The initial data for the considered candidate includes a mass of $\mathrm{M}=1.58\pm0.06\ \mathrm{M}_\odot$ and radius $R=9.1\pm0.4$ km [54]. For this star, the constants (24) and (25) are calculated as $d_1=0.235009$ and $d_2=0.00243166\ \mathrm{km}^{-2}$. Furthermore, a thorough analysis of the model under consideration is conducted, encompassing various properties to assess the validity of the outcomes. We also extend this investigation to assessing the equilibrium as well as stability for the resulting models by considering the parametric range of η, which can either be negative or positive. It must be kept in mind that the plotting is done for multiple choices of the bag constant and identify favorable outcomes when $B_c=90\ \mathrm{MeV/fm}^3$. Therefore, all the plots presented in the following shall correspond to this particular value.

It is crucial to highlight that a valid metric ansatz should not only monotonically increasing function of r but also free from singularities. This is ensured through the plotting of both components given in Eq. (20), as depicted in Fig. 1.

4.1 Matter variables and anisotropy

Ensuring the concentration of fluid within a geometric structure is crucial for validating the resulting solution. It entails that the fluid sector must reach their maximum values and be finitely positive at the center, decreasing outward. To achieve this, we conduct a comparative analysis for models 1 and 2, as illustrated in Fig. 2. Remarkably, the plotting shows that the behavior of the fluid variables aligns with that of physically acceptable interiors. Such an observation provides assistance for the existence of extremely dense interiors within this gravity theory. Upon exploring the first row of Fig. 2, it is guaranteed that the second model produces structures with slightly higher densities. This can also be observed from the numerical values provided in Tables 1 and 2. Furthermore, the subsequent graphs in the same Figure show that model 2 exhibits higher values for pressure components within the stellar body under discussion. Importantly, we also verify the regularity constraints by plotting the first and second derivatives of the fluid variables in Figs. 3 and 4.

Another important factor in the stellar evolution is the pressure anisotropy, and we define it by $\Delta = P_\perp - P_r$ in this case. Here, we shall see how this factor affects the stellar evolutionary pattern through its graphical representation. If the pressure in the tangential direction is higher than the other one, an outward force must occur that prevent the system from collapse. However, the structure is collapse when the radial pressure is much higher than the other component. The expressions for anisotropy corresponding to both models are given in Appendix B. Figure 5 exhibits the plots from where we notice its null profile at the center and consistent increment outwards. We also observe the presence of little more anisotropy in the interior corresponding to the second model.

4.2 Mass function, compactness, redshift and eos parameters

We already defined the mass function in the form of radial metric function (14) in section 2, and it remains the same in this theory as well. However, in this subsection, we define this function in relation with the effective energy density so that the impact of modification of the action (1) can be explored. This is expressed by

$$m(r) = \frac{1}{2}\int_0^R r^2 \mu dr, \tag{26}$$

where the values of μ are presented in Eqs. (16) and (18) analogous to models 1 and 2, respectively. The first two plots of Fig. 6 explains that there is no mass at the center. However, model 2 generates more massive interior of the considered compact star as compared to the other model.

Compactness, specifically, refers to the ratio between an object's mass and its radius. Buchdahl [55], in a seminal contribution, calculated a maximum value for this factor (denoted by β) within the context of a celestial structure, establishing it at $\frac{4}{9}$. A massive object, nestled within a potent gravity field, emits radiations. Such radiations always travel through space, and hence, there occur a stretching in their wavelengths, leading to the redshift phenomenon. Its formula is given as

$$z(r) = \frac{1}{\sqrt{1-2\beta(r)}} - 1. \tag{27}$$

Theoretical models whose interior is configured with uniform distribution typically have a maximum limit of 2 for this parameter. However, an important development came from the contribution of Ivanov [56], who found its value as 5.211 when the anisotropic star is studied. The remaining plots of Fig. 6 confirm both of these factors within their proposed limits.

Furthermore, the EoS is divided into two equations when we are dealing with the anisotropic fluid distribution. They can mathematically be written as

$$\omega_r = \frac{P_r}{\mu}, \quad \omega_\perp = \frac{P_\perp}{\mu}. \tag{28}$$

It must be recalled that both the parameters must remain with the interval [0, 1] to get well-behaved results for the stellar structures. We plot them in Fig. 7, ensuring their required behavior.

4.3 Energy bounds

The internal composition of celestial bodies can consist of either conventional or exotic fluids. Whether a compact star contains a conventional fluid depends on energy conditions determined by physical factors reigning the fluid distribution. When examining astronomical systems within modified theories, it is crucial to account for these conditions, as correction terms can profoundly influence their behavior. Therefore, adhering to the following four types of such conditions ensures the formation of a scientifically valid configuration

- Strong: $\mu + P_r + 2P_\perp \geq 0$,
- Weak: $\mu + P_r \geq 0, \quad \mu \geq 0, \quad \mu + P_\perp \geq 0$,
- Dominant: $\mu \pm P_\perp \geq 0, \quad \mu \pm P_r \geq 0$,
- Null: $\mu + P_\perp \geq 0, \quad \mu + P_r \geq 0$.

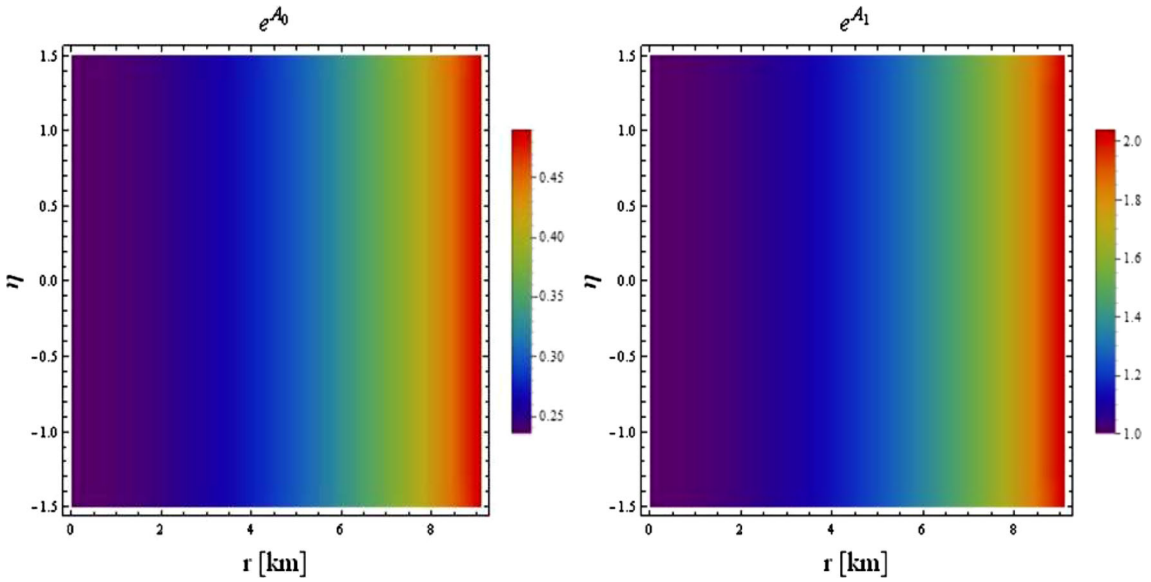

Fig. 1 Metric components (20) versus η and r

Table 1 Numerical values of fluid parameters for 4U 1820-30 corresponding to model 1

Physical Factors	μ_c (g/cm^3)	μ_s (g/cm^3)	P_c (dyne/cm^2)	β_s	z_s
$\eta = -1.5$	1.7138×10^{15}	9.4959×10^{14}	2.4626×10^{35}	0.248	0.909
$\eta = 0$	1.6736×10^{15}	8.9461×10^{14}	2.3267×10^{35}	0.259	1.028
$\eta = 1.5$	1.6295×10^{15}	8.5956×10^{14}	2.2052×10^{35}	0.269	1.147

Table 2 Numerical values of fluid parameters for 4U 1820-30 corresponding to model 2

Physical Factors	μ_c (g/cm^3)	μ_s (g/cm^3)	P_c (dyne/cm^2)	β_s	z_s
$\eta = -1.5$	2.0228×10^{15}	8.4016×10^{14}	2.8678×10^{35}	0.278	0.744
$\eta = 0$	2.0094×10^{15}	1.0727×10^{15}	2.8089×10^{35}	0.284	1.788
$\eta = 1.5$	1.9961×10^{15}	1.4355×10^{15}	2.7115×10^{35}	0.291	0.833

We observe their graphical depiction Figs. 8 and 9. Each plot showcases consistently positive trend, indicating that both of derived solutions meet the standards of physical viability. This suggests the existence of normal matter within their respective interiors.

4.4 Tolman–Opphenheimer–Volkoff equation

Examining various (fundamental) forces is crucial for understanding the evolution of a self-gravitating object. It is essential to assess these forces to determine if the system is in a state of equilibrium or not [57,58]. This can be explored by formulating the Tolman–Oppenheimer–Volkoff (TOV) equation. In the subsequent analysis, we compute the corresponding expression using Eq. (4) for both models as

$$\frac{dP_r}{dr} + \frac{A_0'}{2}(\mu + P_r) - \frac{2}{r}(P_\perp - P_r)$$
$$- \frac{2\eta e^{-A_1}}{\eta\mathcal{R} + 16\pi}$$
$$\times \left[\frac{A_0'\mu}{8}\left(A_0'^2 - A_0'A_1' + 2A_0'' + \frac{4A_0'}{r}\right)\right.$$
$$- \frac{\mu'}{8}\left(A_0'^2 - A_0'A_1' + 2A_0'' - \frac{4A_0'}{r} - \frac{8e^{A_1}}{r^2} + \frac{8}{r^2}\right)$$
$$+ P_r\left(\frac{5A_0'^2A_1'}{8} - \frac{5A_0'A_1'^2}{8} + \frac{7A_0''A_1'}{4}\right.$$
$$- A_0'A_0'' + \frac{A_0'A_1''}{2} - \frac{5A_1'^2}{2r}$$
$$\left. - \frac{A_0'''}{2} + \frac{2A_1''}{r} + \frac{A_0'A_1'}{r} - \frac{A_1'}{r^2} - \frac{A_0''}{r} + \frac{A_0'}{r^2} + \frac{2e^{A_1}}{r^3} - \frac{2}{r^3}\right)$$
$$- \frac{P_r'}{8}\left(A_0'^2 - A_0'A_1' + 2A_0'' - \frac{4A_1'}{r}\right)$$
$$+ \frac{P_\perp}{r^2}\left(A_1' - A_0' + \frac{2e^{A_1}}{r} - \frac{2}{r}\right) - \frac{P_\perp'}{r}\left(\frac{A_1'}{2} - \frac{A_0'}{2}\right.$$
$$\left.\left. + \frac{e^{A_1}}{r} - \frac{1}{r}\right)\right] = 0, \tag{29}$$

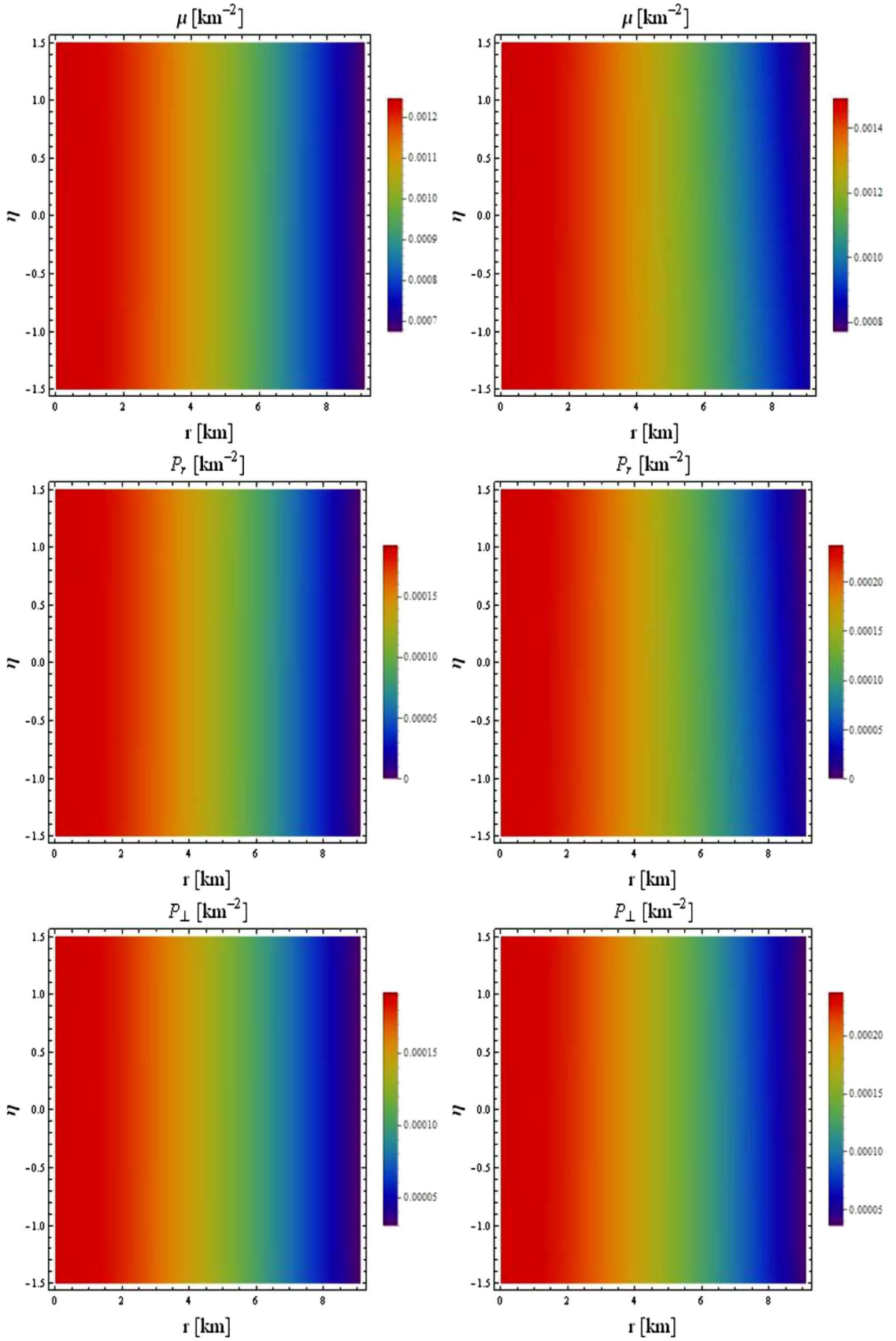

Fig. 2 Matter determinants versus η and r for **Model 1** (left) and **Model 2** (right)

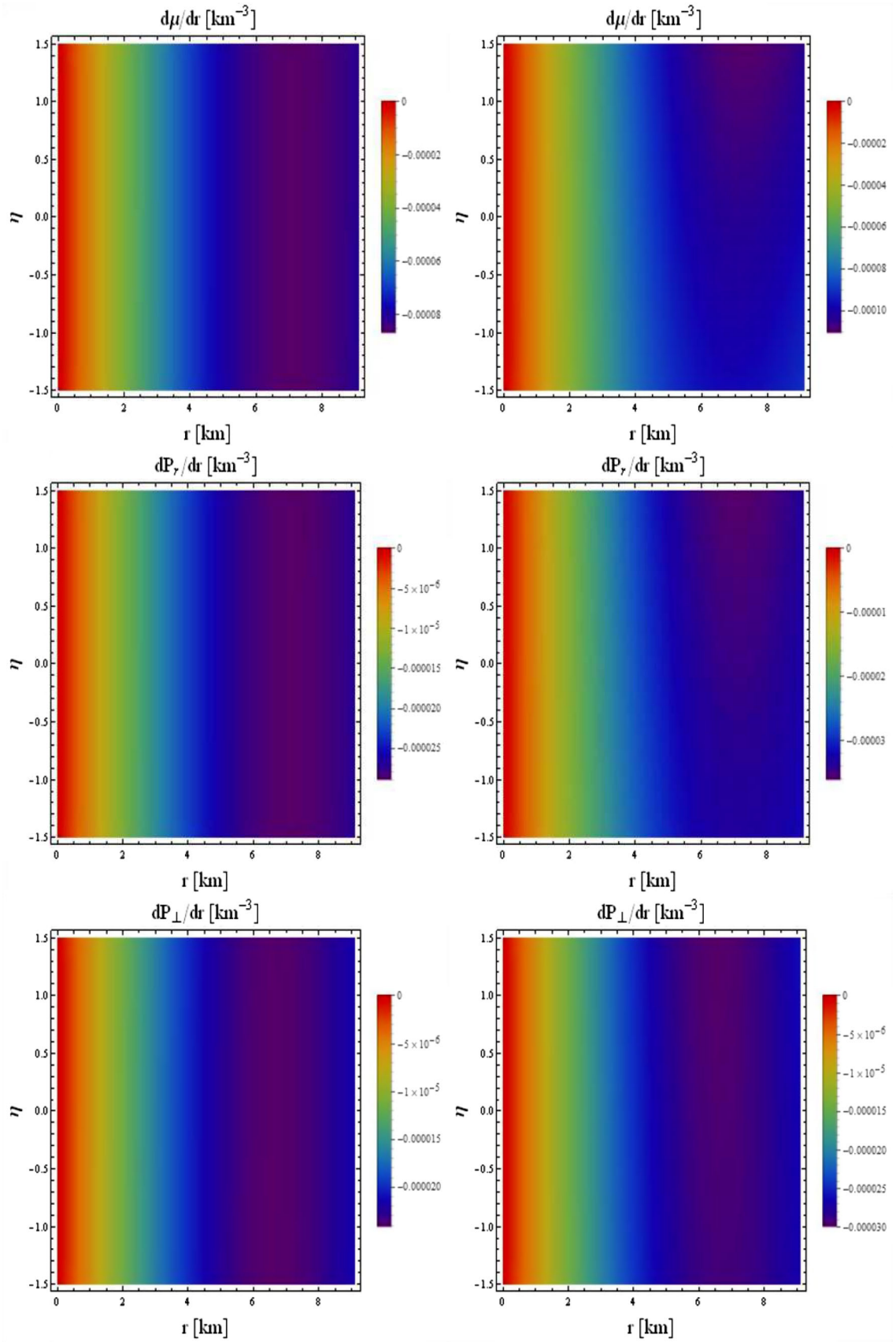

Fig. 3 First-order derivatives of matter determinants versus η and r for **Model 1** (left) and **Model 2** (right)

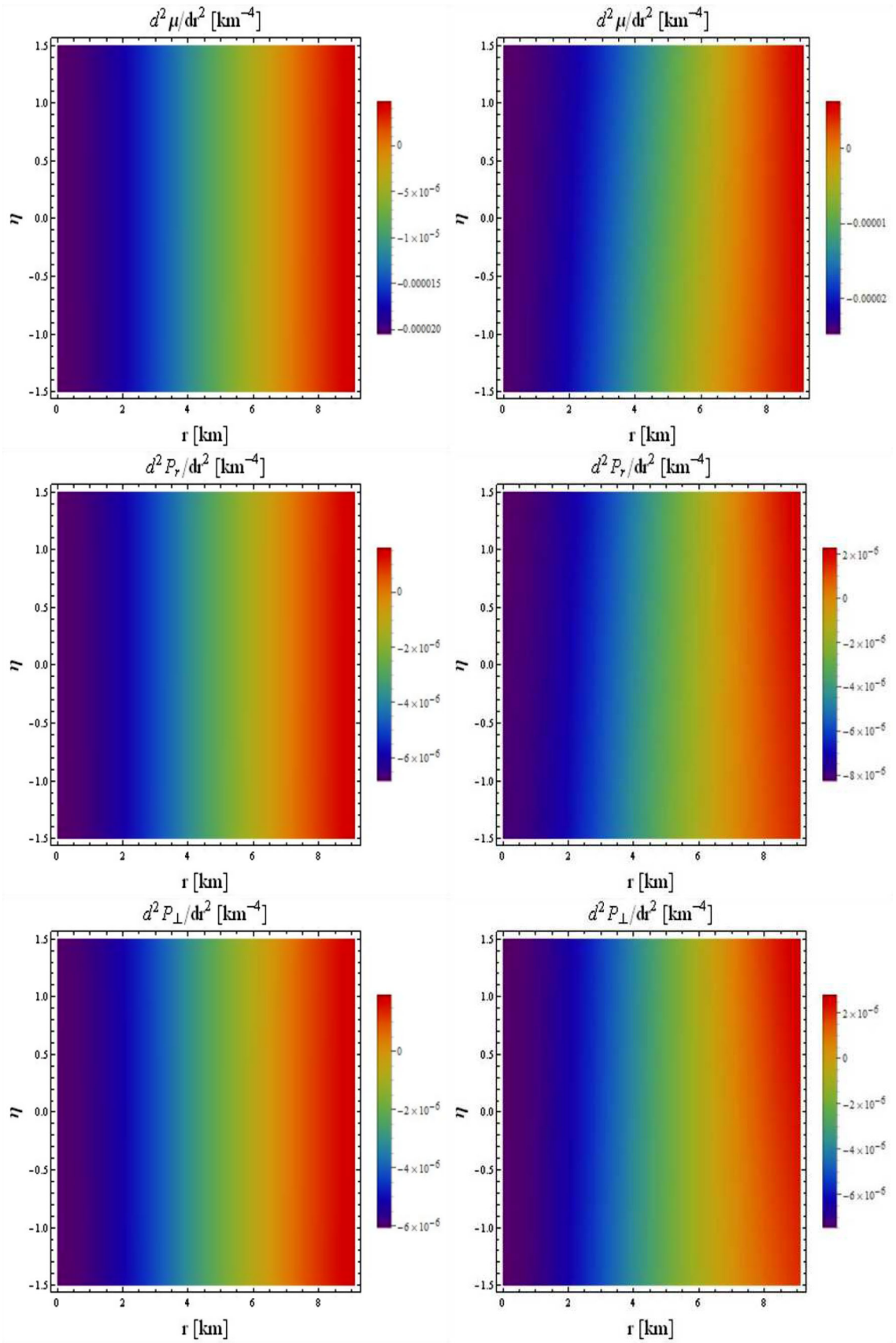

Fig. 4 Second-order derivatives of matter determinants versus η and r for **Model 1** (left) and **Model 2** (right)

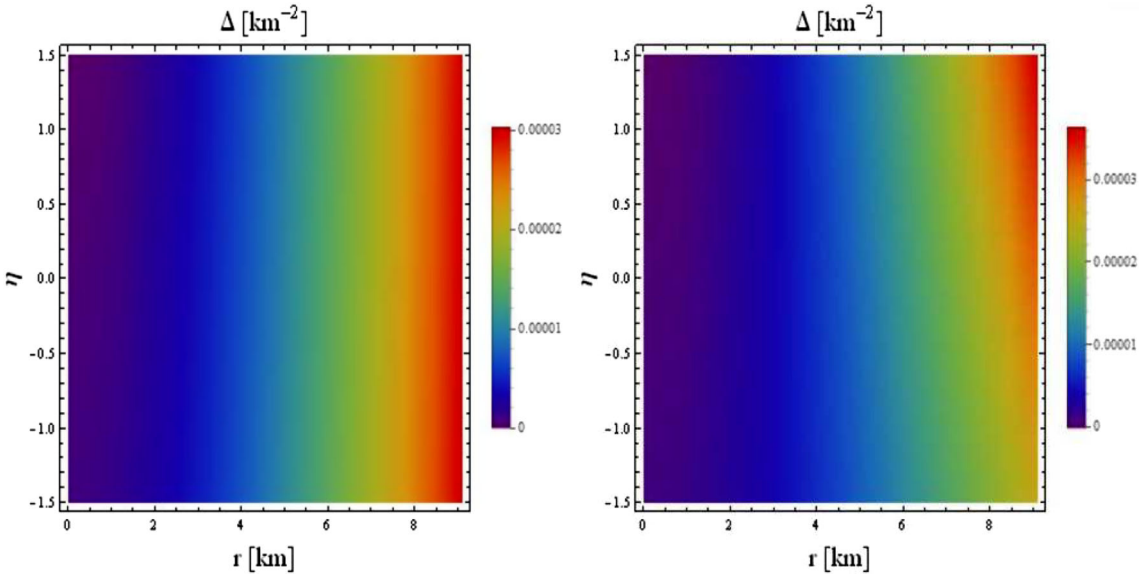

Fig. 5 Anisotropy versus η and r for **Model 1** (left) and **Model 2** (right)

and

$$\frac{dP_r}{dr}+\frac{A_0'}{2}(\mu+P_r)-\frac{2}{r}(P_\perp-P_r)$$
$$-\frac{2\eta}{\eta\mathcal{R}^2+16\pi}\Bigg[\mu\Bigg\{\frac{e^{-A_0-A_1}A_0'\mathcal{R}\mathcal{R}_{00}}{2}-e^{-2A_1}$$
$$\times\mathcal{R}'\left(\frac{A_0'}{r}-\frac{e^{A_1}}{r^2}+\frac{1}{r^2}\right)\Bigg\}$$
$$-\mu'\Bigg\{\frac{e^{-A_0-A_1}\mathcal{R}\mathcal{R}_{00}}{2}-e^{-2A_1}\mathcal{R}\left(\frac{A_0'}{r}-\frac{e^{A_1}}{r^2}+\frac{1}{r^2}\right)\Bigg\}$$
$$+P_r\Bigg\{\mathcal{R}'\mathcal{R}^{11}$$
$$+\mathcal{R}(\mathcal{R}^{11})'-e^{-A_1}\mathcal{R}\mathcal{R}'+\frac{e^{-2A_1}A_1{}'\mathcal{R}\mathcal{R}_{11}}{2}\Bigg\}-\frac{\mathcal{R}\mathcal{R}_{22}}{e^{A_1}}$$
$$\times\left\{\frac{P_t'}{r^2}-\frac{2P_\perp}{r^3}\right\}$$
$$+P_r'\left\{\mathcal{R}\mathcal{R}^{11}-\frac{e^{-2A_1}\mathcal{R}\mathcal{R}_{11}}{2}\right\}\Bigg]=0. \tag{30}$$

The geometric entities ($\mathcal{R}_{00}$, $\mathcal{R}_{11}$ and $\mathcal{R}_{22}$) are expressed in Appendix A. We write the above equations in the concise form as

$$f_{\mathrm{a}}+f_{\mathrm{h}}+f_{\mathrm{y}}=0, \tag{31}$$

with f_{a} being the anisotropic and f_{h} indicates the hydrostatic, defined by

$$f_{\mathrm{a}}=\frac{2}{r}(P_\perp-P_r),\quad f_{\mathrm{h}}=-\frac{dP_r}{dr}.$$

Further, the third entity is the sum of gravitational and an extra force of this gravity theory, i.e., $f_{\mathrm{y}}=f_{\mathrm{g}}+f_{\mathrm{e}}$. This force contains all the remaining terms of (29) and (30) along with a negative sign. These forces are plotted in Fig. 10, guaranteeing the developed interiors to be in hydrostatic equilibrium.

4.5 Stability analysis through different tests

In the expansive domain of cosmic phenomena, significant focus has been directed towards gravitational models that meet stability checks. Various methodologies have been documented to analyze the stability. A crucial approach that often used in such studies is the causality criterion [59,60], which asserts that the speed of light in a stable object must be lower than that of light. Mathematically, we have

$$0<v_{s\perp}^2=\frac{dP_\perp}{d\mu},\quad v_{sr}^2=\frac{dP_r}{d\mu}<1. \tag{32}$$

Herrera [61] put forward this approach and merged both sound speeds into a single expression. He claimed that the absence of cracking can be assured only if $0<\mid v_{s\perp}^2-v_{sr}^2\mid<1$ satisfies, leading to the stability of compact stars. In Fig. 11, we plot all these factors which are found to be within their respective ranges. Hence, our models are stable for every value of η within the chosen range. Another test is named as the adiabatic index, which we denote by Γ, used in the literature regarding stability analysis. According to its definition, both the following components must be greater than $\frac{4}{3}$ [62]. These components are

$$\Gamma_r=\frac{\mu+P_r}{P_r}\left(\frac{dP_r}{d\mu}\right),\Gamma_\perp=\frac{\mu+P_\perp}{P_\perp}\left(\frac{dP_\perp}{d\mu}\right). \tag{33}$$

Both graphs in Fig. 12 satisfy the above-mentioned limit, showing the applicability of the considered modified theory in the framework of anisotropic stellar models.

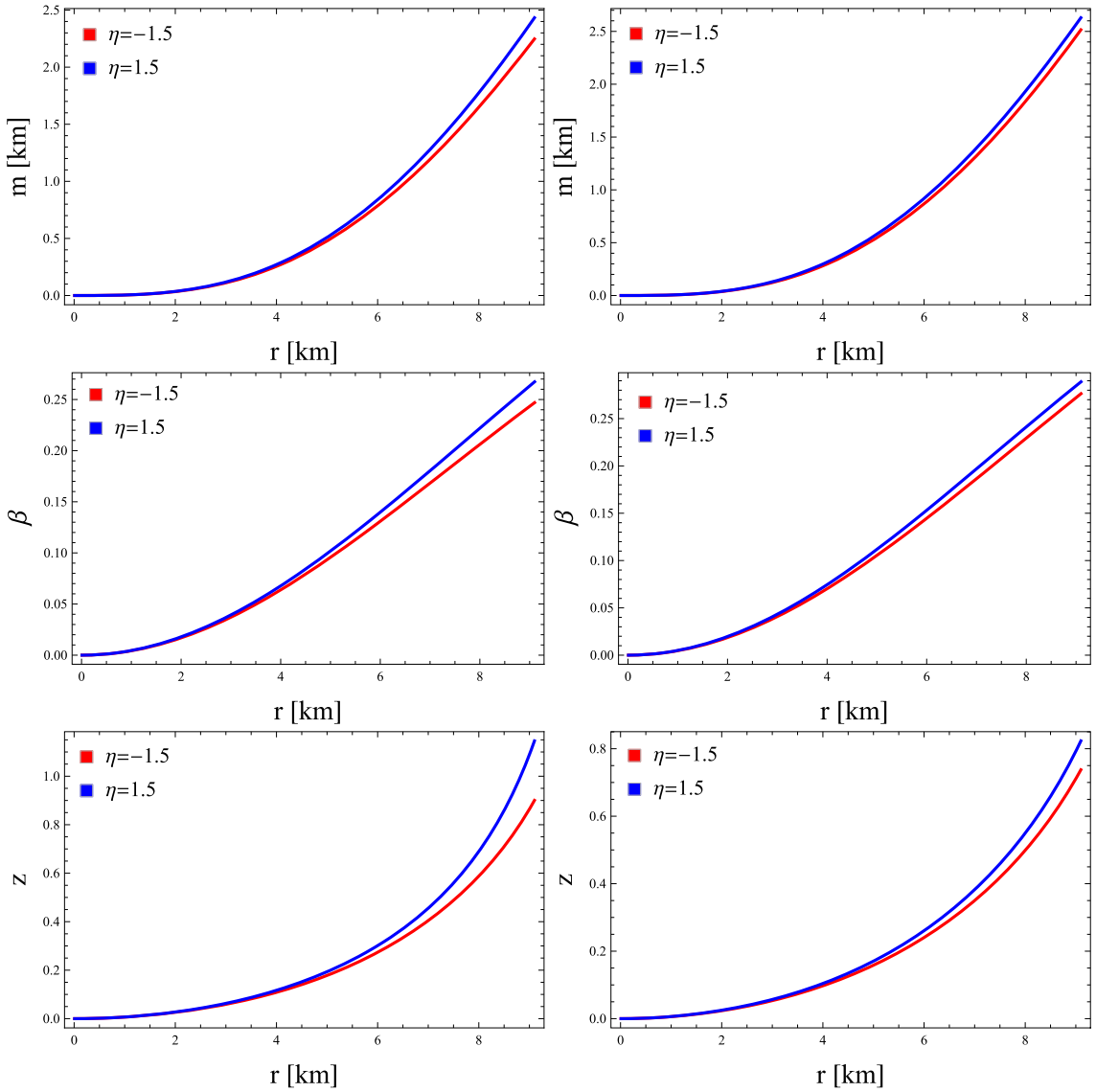

Fig. 6 Physical terms versus η and r for **Model 1** (left) and **Model 2** (right)

5 Finding the model parameter through $P_r \overset{\Sigma}{=} 0$ constraint

The values of the constant η are calculated in this section by using preliminary information of various compact stars. We already used first fundamental form while calculating the doublet (d_1, d_2) in the Durgapal–Fuloria metric (20). Now we use the second form, resulting in the condition on the radial pressure that becomes zero at the interface of any geometrical object, i.e., $P_r \overset{\Sigma}{=} 0$. Implementing this constraint on Eq. (17) corresponding to **Model 1** as, we have

$$
\begin{aligned}
&7\eta \mathrm{M}^2 R\left(79\sqrt{R^5(9R-14\mathrm{M})}+193R^3\right)\\
&\quad-98\eta \mathrm{M}^3\left(6\sqrt{R^5(9R-14\mathrm{M})}+11R^3\right)\\
&\quad-8B_cR^2\left\{56\pi^2R^8-4\pi\eta R^4\left(196\mathrm{M}^2-259\mathrm{M}R+93R^2\right)\right.\\
&\quad+\eta^2\mathrm{M}\left(2744\mathrm{M}^3+31R^3\right.\\
&\quad\left.\left.-3283\mathrm{M}^2R+938\mathrm{M}R^2\right)\right\}\\
&\quad-40\pi R^5\left(\sqrt{R^5(9R-14\mathrm{M})}-3R^3\right)+\mathrm{M}R^2\left\{28\pi\right.\\
&\quad\times\left(3R^2\sqrt{R^5(9R-14\mathrm{M})}-8R^5\right)\\
&\quad\left.-131\eta\sqrt{R^5(9R-14\mathrm{M})}-413\eta R^3\right\}=0. \qquad (34)
\end{aligned}
$$

On the other hand, combining the same condition with (19), we can get the constraints for **Model 2**, which we are left due to a very lengthy expression. However, both constraints are used to find the numerical values of η for different choices of the bag constant corresponsing to **Model 1** and **Model 2**.

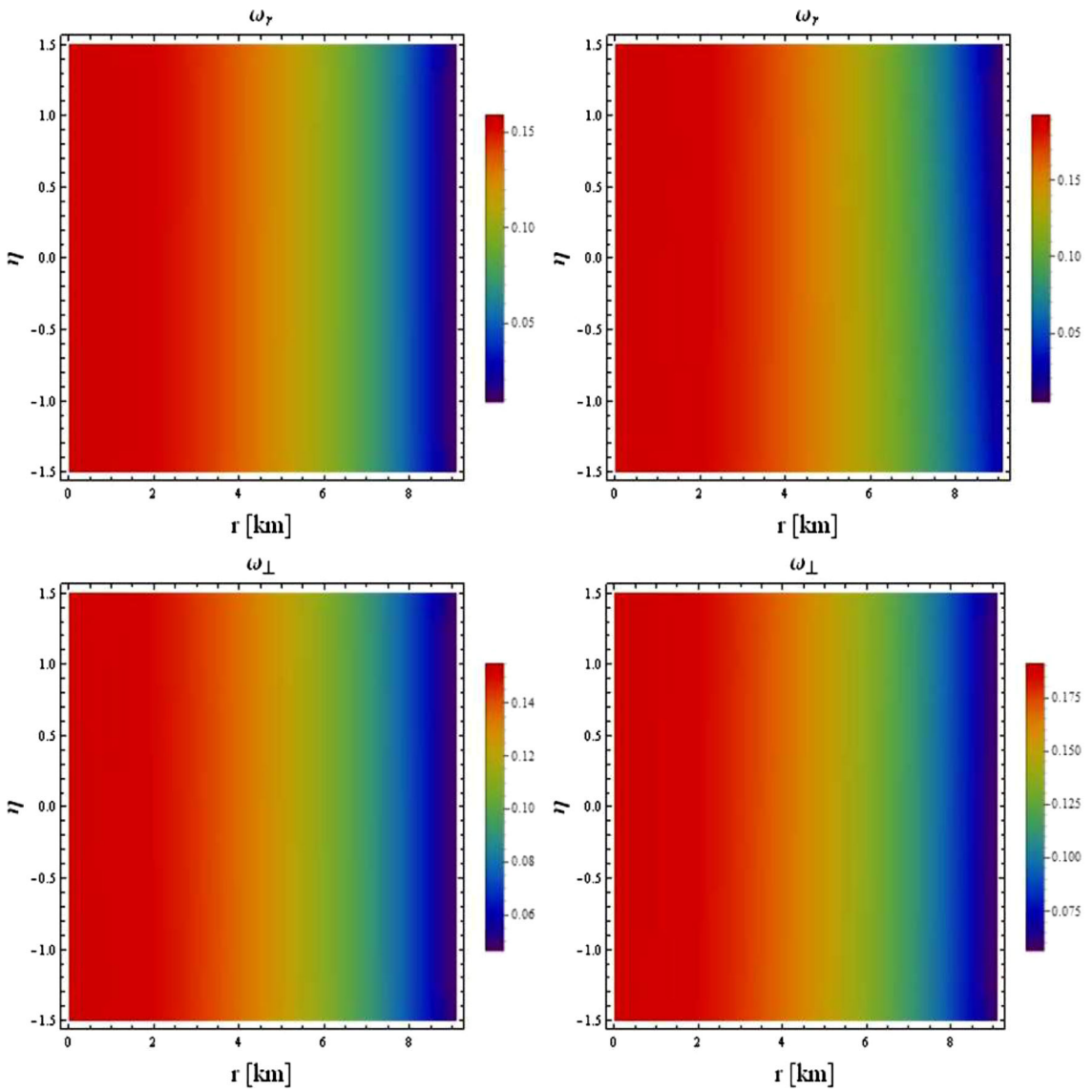

Fig. 7 EoS parameters versus η and r for **Model 1** (left) and **Model 2** (right)

Table 3 Parametric values of η corresponding to model 1

Values of B_c Star candidates	Mass ($M_\odot$)	Radius (km)	73 MeV/fm^3 η	83 MeV/fm^3 η	93 MeV/fm^3 η
Cen X-3	1.49	9.51	− 9.46	3.58	16.45
SMC X-4	1.29	8.83	− 235.61	− 221.391	− 207.36
Her X-1	0.85	8.1	− 826.024	− 525.799	− 288.779
4U 1820-30	1.58	9.1	− 243.39	− 222.84	− 202.57
4U 1608-52	1.74	9.3	− 164.96	− 154.66	− 144.51
PSR J 1614 2230	1.97	10.3	130.28	140.26	143.01
PSR J 1903+327	1.67	9.82	43.32	55.06	66.64
SAX J 1808.4-3658	0.9	7.95	− 447.55	− 428.58	− 209.85

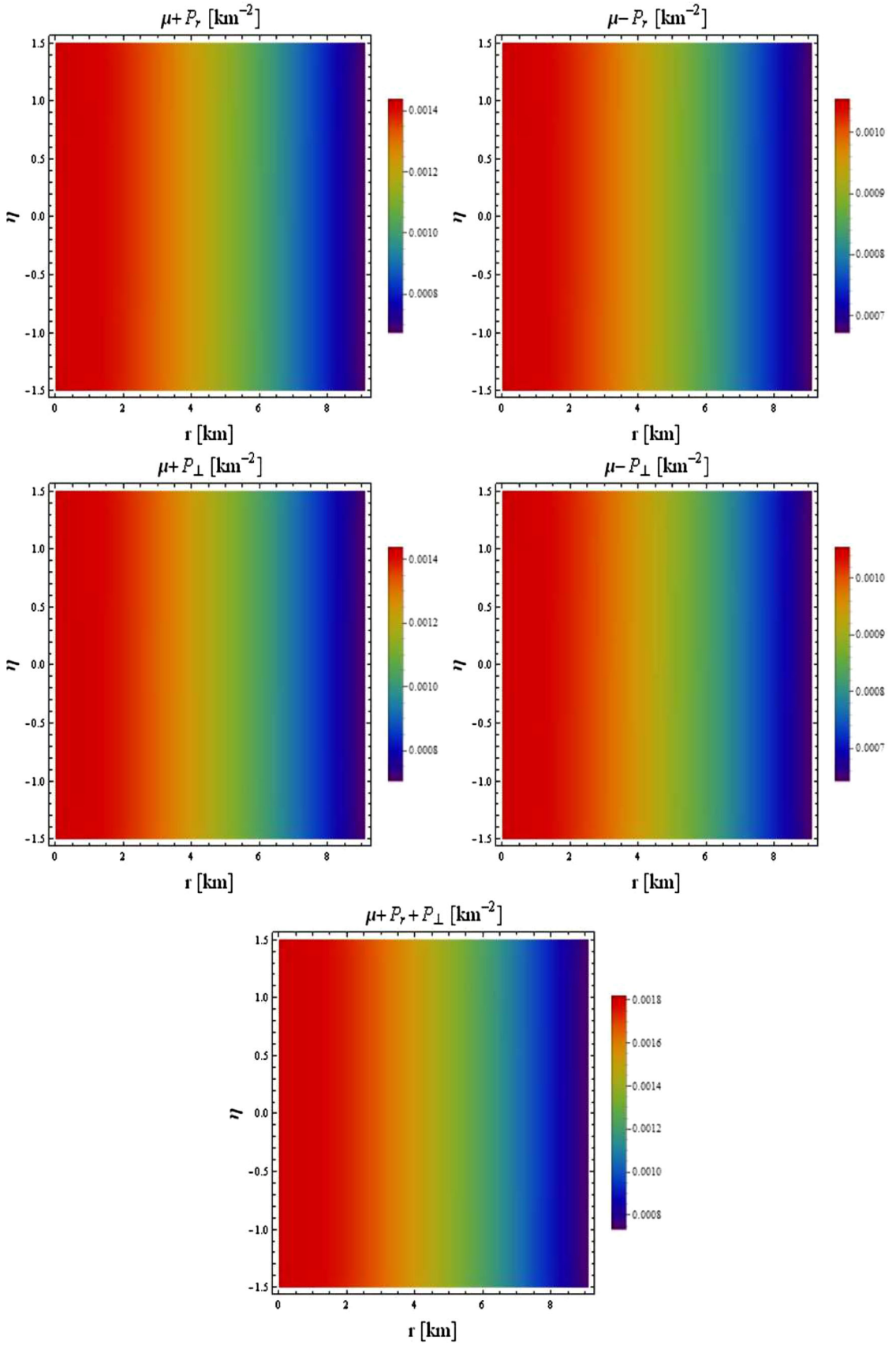

Fig. 8 Energy bounds versus η and r for **Model 1**

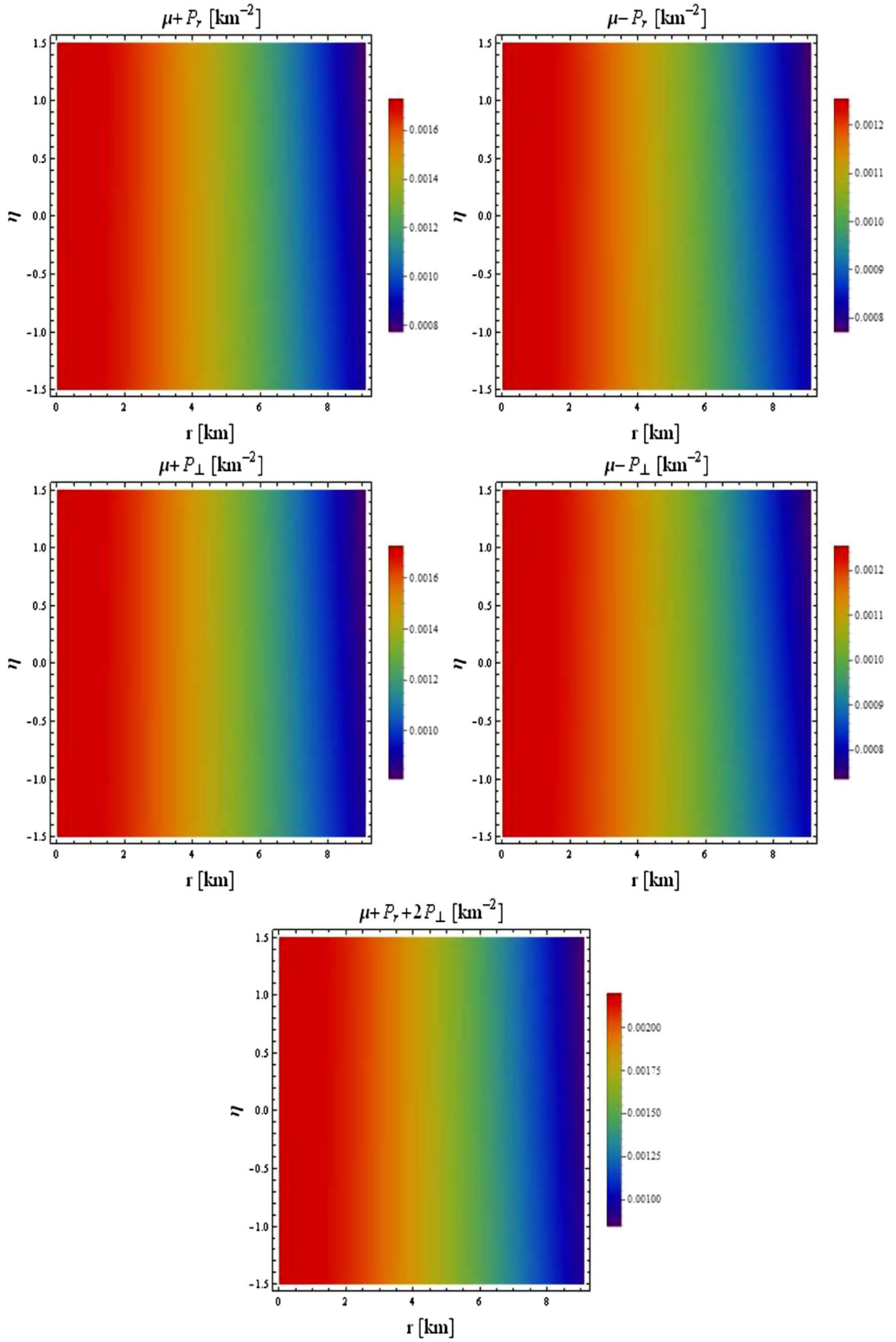

Fig. 9 Energy bounds versus η and r for **Model 2**

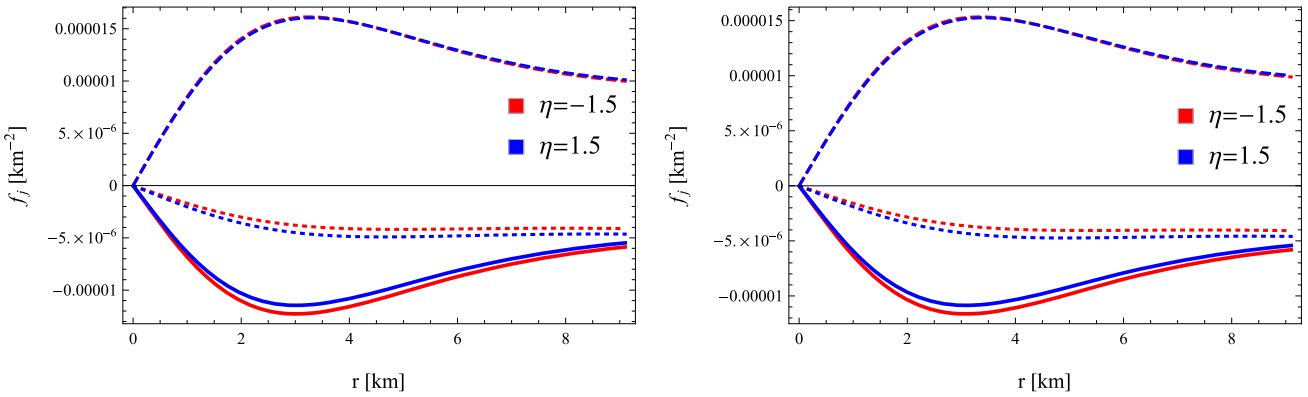

Fig. 10 Variation in f_{a} (solid), f_{h} (dotted) and f_{y} (dashed) versus r for **Model 1** (left) and **Model 2** (right)

Table 4 Parametric values of η corresponding to model 2

Values of B_c Star candidates	Mass ($M_\odot$)	Radius (km)	73 MeV/fm^3 η	83 MeV/fm^3 η	93 MeV/fm^3 η
Cen X-3	1.49	9.51	0.28	−3.36	−6.57
SMC X-4	1.29	8.83	8.24	3.55	−0.57
Her X-1	0.85	8.1	11.25	2.29	−5.58
4U 1820-30	1.58	9.1	6.67	3.31	0.35
4U 1608-52	1.74	9.3	4.82	1.98	−0.51
PSR J 1614 2230	1.97	10.3	−3.11	−5.34	−7.31
PSR J 1903+327	1.67	9.82	−1.17	−4.18	−6.82
SAX J 1808.4-3658	0.9	7.95	20.89	12.54	5.19

We specify their values in Tables 3 and 4, proving η to be a real-valued parameter.

6 Conclusions

This study delves into investigating the existence of different anisotropic compact models within the context of $f(\mathcal{R}, \mathcal{T}, \mathcal{R}_{\zeta\gamma}\mathcal{T}^{\zeta\gamma})$ theory. The consequences of the non-minimal interaction between geometry and matter have been explored by choosing two distinct modified functional forms along with focusing on a specific range of η. We formulated the modified field equations which correspond to the adopted models and identified them as under-determined sets of differential equations possessing high non-linearity. The Durgapal–Fuloria spacetime, meeting specific criteria of acceptability, have been employed to calculate solutions to these equations. Furthermore, the internal structure of strange stars has been described using the MIT bag model. In the context of the Durgapal–Fuloria spacetime, defined by two unknowns (d_1, d_2), calculations have been performed at the hypersurface using matching conditions to determine their values.

Figure 2 exhibited the graphical profile of the matter triplet, ensuring validation of the resulting solutions (for instance, (16), (17) and (18), (19)). Analyzing the mass function within the considered fluid setup indicated itself to be consistently increasing function of the radial coordinate (Fig. 6). It is noted that model 1 displays a less dense interior than model 2 for the specified range of η (Tables 1, 2). Additionally, the graphs depicting compactness and redshift conformed to acceptable ranges. Two parameters related with EoS have been illustrated in Fig. 7, validating the practicality of the constructed models. Throughout the interior, the constraints on EMT take positive values, affirming the physical feasibility of our proposed solutions depicted in Figs. 8 and 9. Furthermore, we have plotted the TOV equations (29) and (30) in Fig. 10, demonstrating that the derived models are in the hydrostatic equilibrium.

Finally, three distinct tests have been utilized to evaluate stability. We have found the stability of the obtained solutions, as evidenced by the observations presented in Figs. 11 and **12**, aligning with the findings in [35,46]. Notably, it is evident that our solutions demonstrated superior efficacy compared to the results obtained in [28], suggesting that the extra force of this extended theory may lead to more favorable outcomes for the specified parametric range. Further, we employed the zero radial pressure constraint at the spherical interface to determine the parameter η that align with the observed masses and radii of an array of compact stars.

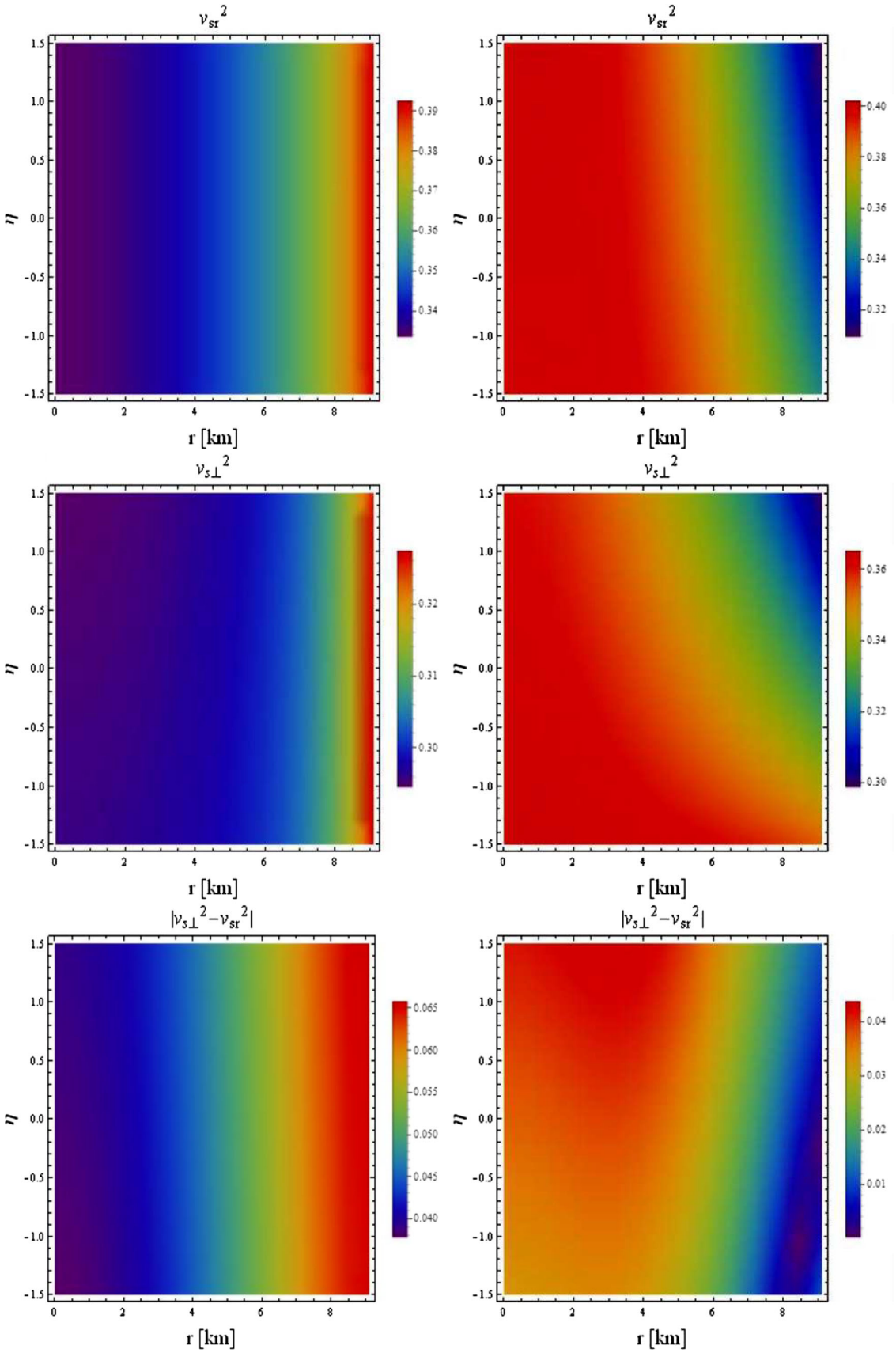

Fig. 11 Stability checks versus η and r for **Model 1** (left) and **Model 2** (right)

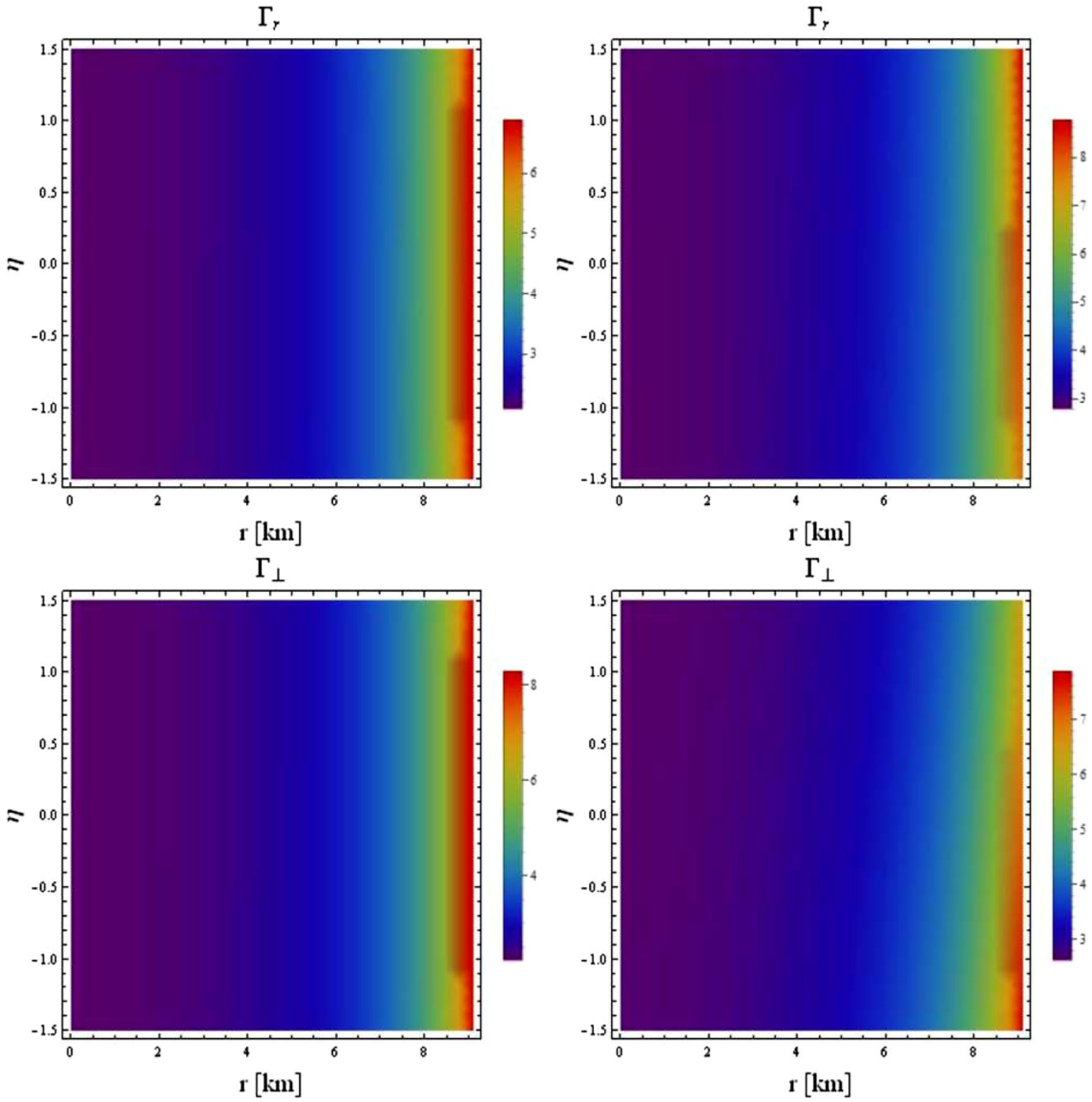

Fig. 12 Adiabatic index versus η and r for **Model 1** (left) and **Model 2** (right)

For models 1 and 2, we have presented these numerical values in Tables 3 and 4, respectively, across various acceptable choices of the bag constant. Notably, η exhibits both negative/positive values, signifying its nature as a real-valued parameter. Ultimately, the parallel results in GR can be found when substituting $\eta = 0$.

Acknowledgements The author SKM is thankful for continuous support and encouragement from the administration of University of Nizwa.

Data Availibility Statement This manuscript has no associated data or the data will not be deposited. [Author[Pleaseinsertintopreamble]s comment: Data sharing not applicable to this article as no datasets were generated or analysed during the current study.]

Code Availibility Statement This manuscript has no associated code/software. [Author's comment: Code/Software sharing not applicable to this article as no code/software was generated or analysed during the current study.]

Funded by SCOAP[3].

Appendix A

The terms $\alpha_j^{'s}$ appeared in Eqs.(11)-(13) are given by

$$\alpha_0 = \frac{e^{-A_1}}{4}\Big(A_0'^2 - A_0'A_1' + 2A_0'' + \frac{4A_0'}{r}\Big),$$
$$\alpha_1 = \frac{e^{-A_1}}{4}\Big(A_0'A_1' - A_0'^2 - 2A_0'' + \frac{4A_1'}{r}\Big),$$
$$\alpha_3 = e^{-A_1}\Big(\frac{A_1'}{r} - \frac{A_0'}{r} + \frac{2e^{A_1}}{r^2} - \frac{2}{r^2}\Big),$$
$$\alpha_4 = \frac{e^{-A_1}}{4}\Big(A_0'A_1'^2 - A_0'^2A_1' - 3A_0''A_1' - A_0'A_1'' + 2A_0'A_0'' + 2A_0''' - \frac{4A_0'}{r^2} - \frac{4A_0'A_1'}{r} + \frac{4A_0''}{r}\Big),$$
$$\alpha_5 = \frac{e^{-A_1}}{4}\Big(A_0'^2A_1' - A_0'A_1'^2 + 3A_0''A_1' + A_0'A_1'' - 2A_0'A_0'' - 2A_0''' - \frac{4A_1'}{r^2} - \frac{4A_1'^2}{r} + \frac{4A_1''}{r}\Big),$$
$$\alpha_6 = e^{-A_1}\Big(\frac{A_0'A_1'}{r} - \frac{4A_1'e^{A_1}}{r^2} - \frac{A_1'^2}{r} + \frac{A_1''}{r} + \frac{A_1'}{r^2} - \frac{A_0''}{r} + \frac{A_0'}{r^2} - \frac{4e^{A_1}}{r^3} + \frac{4}{r^3}\Big),$$
$$\alpha_7 = \frac{e^{-A_1}}{4}\Big(A_0'^2A_1'^2 - A_0'A_1'^3 + 4A_0''A_1'^2 + 3A_0'A_1'A_1'' - 5A_0'''A_1' - 4A_0''A_1'' - A_0'^2A_1'' - A_0'A_1''' - 4A_0'A_0''A_1' + 2A_0''^2 + 2A_0'A_0''' + 2A_0'''' + \frac{4A_0'A_1'^2}{r} - \frac{8A_0''A_1'}{r} - \frac{4A_0'A_1''}{r} + \frac{4A_0'''}{r} - \frac{8A_0''}{r^2} + \frac{8A_0'}{r^3}\Big),$$
$$\alpha_8 = \frac{e^{-A_1}}{4}\Big(A_0'A_1'^3 - A_0'^2A_1'^2 - 4A_0''A_1'^2 - 3A_0'A_1'A_1'' + 4A_0'A_0''A_1' + 5A_0'''A_1' + A_0'^2A_1'' + A_0'A_1''' + 4A_0''A_1'' - 2A_0''^2 - 2A_0'A_0''' - 2A_0'''' + \frac{4A_1'^3}{r} - \frac{12A_1'A_1''}{r} + \frac{8A_1'^2}{r^2} + \frac{4A_1'''}{r} - \frac{8A_1''}{r^2} + \frac{8A_1'}{r^3}\Big),$$
$$\alpha_9 = e^{-A_1}\Big(\frac{A_1'^3}{r} - \frac{A_0'A_1'^2}{r} - \frac{3A_1'A_1''}{r} + \frac{4A_0''A_1'}{r} - \frac{2A_0'A_1'}{r^2} - \frac{6A_1'}{r^3} + \frac{A_0'A_1''}{r} - \frac{A_1''e^{A_1}}{r^2} + \frac{8A_1'e^{A_1}}{r^3} + \frac{A_1'''}{r} - \frac{A_0'''}{r} + \frac{2A_0''}{r^2} - \frac{2A_0'}{r^3} + \frac{12e^{A_1}}{r^4} - \frac{12}{r^4}\Big).$$

The geometric terms for the line element (6) are

$$\mathcal{R} = \frac{1}{2e^{A_1}}\Big(A_0'^2 - A_1'A_0' + 2A_0'' - \frac{4A_1'}{r} + \frac{4A_0'}{r} - \frac{4e^{A_1}}{r^2} + \frac{4}{r^2}\Big),$$
$$\mathcal{R}_{00} = \frac{1}{4e^{A_1-A_0}} \times \Big(A_0'^2 - A_1'A_0' + 2A_0'' + \frac{4A_0'}{r}\Big),$$
$$\mathcal{R}_{11} = \frac{1}{4}\Big(A_1'A_0' - A_0'^2 - 2A_0'' + \frac{4A_1'}{r}\Big), \quad \mathcal{R}_{22} = \frac{1}{2e^{A_1}}\Big(A_1'r - A_0'r + 2e^{A_1} - 2\Big).$$

Appendix B

The anisotropic factor analogous to model 1 is

$$\Delta = \Big\{\big(2\eta r A_0'' - \eta A_1'(rA_0' + 4) + \eta r A_0'^2 + 4\eta A_0' + 32\pi r e^{A_1}\big)\big(2\big(8\eta - \eta r^2 A_1'' + 9\eta r^2 A_0'' + 64\pi r^2 e^{A_1} - 8\eta e^{A_1}\big) - \eta r^2 A_1'^2 + r^2 3\eta A_0'^2 - 10\eta r A_1'(rA_0' + 4) + 16\eta r A_0'\big)\Big\}^{-1}\Big\{3\eta r^3(6\eta B_c + 1)A_0'^4 + 4r\big(\eta A_1''\big(8B_c\big(\eta + \big(8\pi r^2 - \eta\big)e^{A_1}\big) + r^2 \times (4\eta B_c - 1)A_0''\big) + 8A_0''\big(\eta(1 + \eta B_c) + e^{A_1}\big(8\pi r^2(3\eta B_c + 1) - \eta(\eta B_c + 1)\big)\big) + 128\pi B_c e^{A_1}\big(\big(8\pi r^2 - \eta\big)e^{A_1} + \eta\big) + \eta r^2(10\eta B_c + 9)A_0''^2\big) + 2rA_0'^2\big(4\big(2\big(2\eta \times (3\eta B_c + 1) + (2B_c\eta + 1)\big(8\pi r^2 - \eta\big)e^{A_1}\big) + \eta r^2(7\eta B_c + 3)A_0''\big) - \eta r^2 A_1'' \times (6\eta B_c + 1)\big) + 4A_0'\big(8\big(\eta(2\eta B_c + 1) + e^{A_1}\big(4\pi r^2(8\eta B_c + 1) - \eta(2\eta B_c + 1)\big)\big) + r^2(24\eta B_c + 19)\eta A_0'' - 3\eta r^2 A_1''\big) + \eta r^2 A_1'^3\big(88\eta B_c + (22\eta B_c r + r)A_0' + 14\big) + \eta r A_1'^2\big(-2\big(8\big(B_c\big(\eta + 24\pi r^2\big)e^{A_1} - 9\eta B_c - 4\big) + (22\eta B_c + 1)A_0''(r)r^2\big) + 9r^2 \times A_0'^2(2\eta B_c + 1) + 6r(8\eta B_c + 11)A_0'\big) + 2\eta r^2(16\eta B_c + 19)A_0'^3 - A_1'\big(\eta r^3 A_0'^3$$

$$\times (34\eta B_c + 13) + 4\big(\eta r^2(12\eta B_c + 1)A_1{}'' + 8\big(\eta(2\eta B_c + 1) - e^{A_1}\big(\eta(1 + 2\eta B_c) - 12\pi r^2(4\eta B_c + 1)\big)\big) + \eta r^2(44\eta B_c + 27)A_0''\big) + 2rA_0'\big(\eta r^2(6\eta B_c - 1)A_1{}'' + 8 \times \big(\eta(13\eta B_c + 10) + e^{A_1}\big(8\pi r^2(3\eta B_c + 1) - \eta(\eta B_c + 1)\big)\big) + \eta(22\eta B_c + 19) \times r^2A_0''\big) + 2\eta r^2(92\eta B_c + 35)A_0'^2\big)\Big\},$$

while its value for model 2 is

$$\Delta = \Big\{2e^{A_1}r^2\eta\mathcal{R}^2 + 4\eta\big(rA_1{}' + 2e^{A_1} - rA_0' - 2\big)\mathcal{R} + r\big(\eta\big(r\mathcal{R}' - 2r\alpha_6 - 4\alpha_3\big)A_0' - r\eta\alpha_3A_0'^2 + 32e^{A_1}\pi r - 4r\eta\alpha_9 - 4\eta\alpha_6 + \eta A_1{}'\big(rA_0'\alpha_3 + 4\alpha_3 + 2r\alpha_6 - r\mathcal{R}'\big) + 2r \times \eta\mathcal{R}'' - 2r\eta\alpha_3A_0''\big)\Big\}^{-1} \Big\{r\big(rA_0'^2 + 2A_0' - A_1{}'\big(rA_0' + 2\big) + 2rA_0''\big)\Big\} + \Big\{8e^{A_1}r\eta\mathcal{R}^2 + \eta\big(A_1{}'\big(7rA_0' - 4\big) - rA_0'^2 - 20A_0' - 8rA_0''\big)\mathcal{R} + 2\big(2\eta\alpha_8r - 3\eta\alpha_4A_0'r - \eta\alpha_5A_0'r + 2\eta\mathcal{R}''r + 64e^{A_1}\pi r - \eta(6\alpha_1 + 2\alpha_2 + 3r\alpha_4 + r\alpha_5)A_1{}' - \eta\mathcal{R}'\big(rA_1{}' + rA_0' - 4\big) - 6\eta\alpha_1A_0' - 2\eta\alpha_2A_0'\big)\Big\}^{-1} \times \Big\{4\big(2e^{A_1}r\eta B_c\mathcal{R}^2 + \eta B_c\big(2A_1{}'\big(rA_0' - 2\big) - rA_0'^2 - 8A_0' - 2rA_0''\big)\mathcal{R} + 32e^{A_1}\pi rB_c + 4r\eta B_c\alpha_7 - 4\eta B_c\alpha_1A_1{}' - 2r\eta B_c\alpha_4A_1{}' - A_1{}' - 4\eta B_c\alpha_1 \times A_0' - 2r\eta B_c\alpha_4A_0' - A_0' - \eta B_cR'\big(rA_1{}' + rA_0' - 4\big) + 2r\eta B_c\mathcal{R}''\big)\Big\} + \Big\{\big(8e^{A_1}r\eta\mathcal{R}^2 + \eta\big(-rA_0'^2 - 20A_0' + A_1{}'\big(7rA_0' - 4\big) - 8rA_0''\big)\mathcal{R} + 2\big(2\eta\alpha_8r - 3\eta\alpha_4A_0'r - \eta\alpha_5A_0'r + 2\eta\mathcal{R}''r + 64e^{A_1}\pi r - \eta(6\alpha_1 + 2\alpha_2 + 3r\alpha_4 + r\alpha_5)A_1{}' - 6\eta\alpha_1A_0' - 2\eta\alpha_2A_0' - \eta\mathcal{R}' \times \big(rA_1{}' + rA_0' - 4\big)\big)\big)\big(2e^{A_1}r^2\eta\mathcal{R}^2 + 4\eta\big(rA_1{}' + 2e^{A_1} - rA_0' - 2\big)\mathcal{R} - r\big(r\eta\alpha_3A_0'^2 - \eta\big(-4\alpha_3 - 2r\alpha_6 + r\mathcal{R}'\big)A_0' - 32e^{A_1}\pi r + 4r\eta\alpha_9 + 4\eta\alpha_6 - \eta A_1{}'\big(rA_0'\alpha_3 + 2r\alpha_6 + 4\alpha_3 - r\mathcal{R}'\big) - 2r\eta\mathcal{R}'' + 2r\eta\alpha_3A_0''\big)\Big\}^{-1} \Big\{2r\eta\big(\big(-r(2\alpha_1 + \mathcal{R})A_0'^2 - \big(4\alpha_1 + r4\alpha_4 - 2r\mathcal{R}'\big)A_0' - 8r\alpha_7 - 8\alpha_4 + A_1{}'\big(2rA_0'\alpha_1 + 4\alpha_1 + 4r\alpha_4 + \mathcal{R}\big(rA_0' + 4\big)\big) - r4\alpha_1A_0'' - 2r\mathcal{R}A_0''\big)\big(2e^{A_1}r\eta B_c\mathcal{R}^2 + \eta B_c\big(2rA_0'^2 + 4A_0' + A_1{}'\big(rA_0' + 8\big) - 2rA_0''\big)\mathcal{R} - 3A_1{}' - 32e^{A_1}\pi rB_c + 4r\eta B_c\alpha_8 - 4\eta B_c\alpha_2A_1{}' - 2r\eta B_c\alpha_5A_1{}' - 4\eta B_c\alpha_2A_0' - 2r\eta\alpha_5B_cA_0' - 3A_0' + \eta B_c\mathcal{R}'\big(rA_1{}' + rA_0' - 4\big) - 2r\eta B_c\mathcal{R}''\big) + \big(2r\alpha_2A_0'^2 - r\mathcal{R}A_0'^2 + 4\alpha_2A_0' + 8\alpha_5 + 4r\alpha_5A_0' - 4\mathcal{R}A_0' + 8r\alpha_8 + 2\mathcal{R}'\big(rA_1{}' - 2rA_0' - 4\big) + \big((\mathcal{R} - 2\alpha_2)rA_0' - 4(\alpha_2 + r\alpha_5)\big) \times A_1{}' - 4r\mathcal{R}'' + 4r\alpha_2A_0'' - 2r\mathcal{R}A_0''\big)\big(-2e^{A_1}r\eta B_c\mathcal{R}^2 + \eta B_c\big(A_0'^2r + 8A_0' + 2rA_0'' + A_1{}'\big(4 - 2rA_0'\big)\big)\mathcal{R} - 32e^{A_1}\pi rB_c - 4r\eta B_c\alpha_7 + 4\eta B_c\alpha_1A_1{}' + 2r\eta B_c\alpha_4A_1{}' + A_1{}' + 4\eta B_c\alpha_1A_0' + 2r\eta B_c\alpha_4A_0' + A_0' + \eta B_c\mathcal{R}'\big(rA_1{}' + rA_0' - 4\big) - 2r\eta B_c\mathcal{R}''\big)\big)\Big\}.$$

References

1. H.A. Buchdahl, Non-linear Lagrangians and cosmological theory. Mon. Not. R. Astron. Soc. **150**, 1–8 (1970)
2. S. Nojiri, S.D. Odintsov, Modified gravity with negative and positive powers of curvature: unification of inflation and cosmic acceleration. Phys. Rev. D **68**, 123512 (2003)
3. Y.S. Song, W. Hu, I. Sawicki, Large scale structure of $f(R)$ gravity. Phys. Rev. D **75**, 044004 (2007)
4. A.V. Astashenok, S. Capozziello, S.D. Odintsov, Maximal neutron star mass and the resolution of the hyperon puzzle in modified gravity. Phys. Rev. D **89**, 103509 (2014)
5. G. Mustafa, I. Hussain, M.F. Shamir, Stable wormholes in the background of an exponential $f(R)$ gravity. Universe **6**, 48 (2020)
6. M.F. Shamir, A. Malik, G. Mustafa, Noncommutative wormhole solutions in modified $f(R)$ theory of gravity. Chin. J. Phys. **73**, 634 (2021)
7. S. Capozziello, S. Nojiri, S.D. Odintsov, A. Troisi, Cosmological viability of $f(R)$-gravity as an ideal fluid and its compatibility with a matter dominated phase. Phys. Lett. B **639**, 135 (2006)
8. J.D. Barrow, S. Hervik, Anisotropically inflating universes. Phys. Rev. D **73**, 023007 (2006)
9. M. Visser, Energy conditions in the epoch of galaxy formation. Science **276**, 88 (1997)
10. T. Naseer, M. Sharif, Implications of vanishing complexity condition in $f(R)$ theory. Eur. Phys. J. C **84**, 554 (2024)
11. O. Bertolami, C.G. Boehmer, T. Harko, F.S.N. Lobo, Extra force in $f(R)$ modified theories of gravity. Phys. Rev. D **75**, 104016 (2007)
12. T. Harko, F.S.N. Lobo, S. Nojiri, S.D. Odintsov, $f(R, T)$ gravity. Phys. Rev. D **84**, 024020 (2011)

13. M. Sharif, M. Zubair, Thermodynamic behavior of particular $f(R,T)$-gravity models. J. Exp. Theor. Phys. **117**, 248–257 (2013)
14. H. Shabani, M. Farhoudi, $f(R,T)$ cosmological models in phase space. Phys. Rev. D **88**, 044048 (2013)
15. A. Das, S. Ghosh, B.K. Guha, S. Das, F. Rahaman, S. Ray, Gravastars in $f(R,T)$ gravity. Phys. Rev. D **95**, 124011 (2017)
16. S.K. Maurya, A. Banerjee, F. Tello-Ortiz, Buchdahl model in $f(R,T)$ gravity: a comparative study with standard Einstein's gravity. Phys. Dark Universe **27**, 100438 (2020)
17. G. Mustafa, M. Zubair, S. Waheed, X. Tiecheng, Realistic stellar anisotropic model satisfying Karmarker condition in $f(R,T)$ gravity. Eur. Phys. J. C **80**, 26 (2020)
18. P. Rej, P. Bhar, Charged strange star in $f(R,T)$ gravity with linear equation of state. Astrophys. Space Sci. **366**, 35 (2021)
19. A. Errehymy, Y. Khedif, G. Mustafa, M. Daoud, Anisotropic stars of class one space-time in $f(R,T)$ gravity under the simplest linear functional of the matter-geometry coupling. Chin. J. Phys. **77**, 1502 (2022)
20. M. Sharif, T. Naseer, Anisotropic complexity-free models in modified $f(R,T)$ theory. Ann. Phys. **459**, 169527 (2023)
21. M. Sharif, T. Naseer, Effect of extended gravitational decoupling on isotropization and complexity in $f(R,T)$ theory. Class. Quantum Gravity **40**, 035009 (2023)
22. T. Naseer, M. Sharif, Study of decoupled cosmological solutions in $f(R,T)$ theory. Fortschr. Phys. **71**, 2300004 (2023)
23. Z. Haghani, T. Harko, F.S.N. Lobo, H.R. Sepangi, S. Shahidi, Further matters in space-time geometry: $f(R,T,R_{\mu\nu}T^{\mu\nu})$ gravity. Phys. Rev. D **88**, 044023 (2013)
24. M. Sharif, M. Zubair, Study of thermodynamic laws in $f(R,T,R_{\mu\nu}T^{\mu\nu})$ gravity. J. Cosmol. Astropart. Phys. **11**, 042 (2013)
25. S.D. Odintsov, D. Sáez-Gómez, $f(R,T,R_{\mu\nu}T^{\mu\nu})$ gravity phenomenology and ΛCDM universe. Phys. Lett. B **725**, 437–444 (2013)
26. I. Ayuso, J.B. Jiménez, Á. De la Cruz-Dombriz, Consistency of universally nonminimally coupled $f(R,T,R_{\mu\nu}T^{\mu\nu})$ theories. Phys. Rev. D **91**, 104003 (2015)
27. E.H. Baffou, M.J.S. Houndjo, J. Tosssa, Exploring stable models in $f(R,T,R_{\mu\nu}T^{\mu\nu})$ gravity. Astrophys. Space Sci. **361**, 376 (2016)
28. M. Sharif, A. Waseem, Physical behavior of anisotropic compact stars in $f(R,T,R_{\mu\nu}T^{\mu\nu})$ gravity. Can. J. Phys. **94**, 1024–1039 (2016)
29. Z. Yousaf, M.Z. Bhatti, T. Naseer, Study of static charged spherical structure in $f(R,T,Q)$ gravity. Eur. Phys. J. Plus **135**, 353 (2020)
30. Z. Yousaf, M.Z. Bhatti, T. Naseer, Measure of complexity for dynamical self-gravitating structures. Int. J. Mod. Phys. D **29**, 2050061 (2020)
31. Z. Yousaf et al., The measure of complexity in charged celestial bodies in $f(R,T,R_{\mu\nu}T^{\mu\nu})$ gravity. Phys. Dark Universe **29**, 100581 (2020)
32. Z. Yousaf, M.Z. Bhatti, T. Naseer, Evolution of the charged dynamical radiating spherical structures. Ann. Phys. **420**, 168267 (2020)
33. Z. Yousaf, M.Z. Bhatti, T. Naseer, New definition of complexity factor in $f(R,T,R_{\mu\nu}T^{\mu\nu})$ gravity. Phys. Dark Universe **28**, 100535 (2020)
34. Z. Yousaf et al., Influence of modification of gravity on the complexity factor of static spherical structures. Mon. Not. R. Astron. Soc. **495**, 4334–4346 (2020)
35. T. Naseer, M. Sharif, A. Fatima, S. Manzoor, Constructing traversable wormhole solutions in $f(R,L_m)$ theory. Chin. J. Phys. **86**, 350 (2023)
36. M. Sharif, T. Naseer, Study of charged compact stars in nonminimally coupled gravity. Fortschr. Phys. **71**, 2200147 (2023)
37. B. Das, P.C. Ray, I. Radinschi, F. Rahaman, S. Ray, Isotropic cases of static charged fluid spheres in general relativity. Int. J. Mod. Phys. D **20**, 1675 (2011)
38. G.H. Bordbar, A.R. Peivand, Computation of the structure of a magnetized strange quark star. Res. Astron. Astrophys. **11**, 851 (2011)
39. P. Haensel, J.L. Zdunik, R. Schaefer, Strange quark stars. Astron. Astrophys. **160**, 121 (1986)
40. K.S. Cheng, Z.G. Dai, T. Lu, Strange stars and related astrophysical phenomena. Int. J. Mod. Phys. D **7**, 139 (1998)
41. M.K. Mak, T. Harko, An exact anisotropic quark star model. Chin. J. Astron. Astrophys. **2**, 248 (2002)
42. P. Rej, P. Bhar, Model of hybrid star with baryonic and strange quark matter in Tolman–Kuchowicz spacetime. Int. J. Geom. Methods Mod. **19**, 2250104 (2022)
43. P. Rej, A. Errehymy, M. Daoud, Charged strange star model in Tolman–Kuchowicz spacetime in the background of 5D Einstein–Maxwell–Gauss–Bonnet gravity. Eur. Phys. J. C **83**, 392 (2023)
44. P.B. Demorest, T. Pennucci, S.M. Ransom, M.S.E. Roberts, J.W.T. Hessels, A two-solar-mass neutron star measured using Shapiro delay. Nature **467**, 1081 (2010)
45. F. Rahaman, K. Chakraborty, P.K.F. Kuhfittig, G.C. Shit, M. Rahman, A new deterministic model of strange stars. Eur. Phys. J. C **74**, 3126 (2014)
46. M.R. Shahzad, G. Abbas, Strange stars with MIT bag model in the Rastall theory of gravity. Int. J. Geom. Methods Mod. Phys. **16**, 1950132 (2019)
47. A. Errehymy, A. Ditta, G. Mustafa, S.K. Maurya, A. Abdel-Aty, Anisotropic electrically charged stars in $f(Q)$ symmetric teleparallel gravity. Eur. Phys. J. Plus **137**, 1311 (2022)
48. C.W. Misner, D.H. Sharp, Relativistic equations for adiabatic, spherically symmetric gravitational collapse. Phys. Rev. **136**, B571 (1964)
49. M. Kalam, A.A. Usmani, F. Rahaman, S.M. Hossein, I. Karar, R. Sharma, A relativistic model for strange quark star. Int. J. Theor. Phys. **52**, 3319 (2013)
50. J.D.V. Arbañil, M. Malheiro, Radial stability of anisotropic strange quark stars. J. Cosmol. Astropart. Phys. **11**, 012 (2016)
51. T. Naseer, M. Sharif, S. Manzoor, A. Fatima, Anisotropic Durgapal–Fuloria neutron stars in $f(R,T^2)$ gravity. Mod. Phys. Lett. A **39**, 2450048 (2024)
52. K. Lake, All static spherically symmetric perfect-fluid solutions of Einstein's equations. Phys. Rev. D **67**, 104015 (2003)
53. T. Naseer, M. Sharif, Estimating the role of bag constant and modified theory on anisotropic stellar models. Chin. J. Phys. **88**, 10–31 (2024)
54. T. Güver, P. Wroblewski, L. Camarota, F. Özel, The mass and radius of the neutron star in 4U 1820-30. Astrophys. J. **719**, 1807 (2010)
55. H.A. Buchdahl, General relativistic fluid spheres. Phys. Rev. **116**, 1027 (1959)
56. B.V. Ivanov, Maximum bounds on the surface redshift of anisotropic stars. Phys. Rev. D **65**, 104011 (2002)
57. F. Tello-Ortiz, S.K. Maurya, Y. Gomez-Leyton, Class I approach as MGD generator. Eur. Phys. J. C **80**, 324 (2020)
58. B. Dayanandan, T.T. Smitha, S.K. Maurya, Self-gravitating anisotropic star using gravitational decoupling. Phys. Scr. **96**, 125041 (2021)
59. H. Abreu, H. Hernandez, L.A. Nunez, Sound speeds, cracking and the stability of self-gravitating anisotropic compact objects. Class. Quantum Gravity **24**, 4631 (2007)
60. T. Naseer, M. Sharif, Decoupled anisotropic Buchdahl's relativistic models in $f(R,T)$ theory. Phys. Scr. **99**, 035001 (2024)
61. L. Herrera, Cracking of self-gravitating compact objects. Phys. Lett. A **165**, 206 (1992)
62. H. Heintzmann, W. Hillebrandt, Neutron stars with an anisotropic equation of state—mass, redshift and stability. Astron. Astrophys. **38**, 51–55 (1975)